Joint Transmit Designs for Co-existence of MIMO Wireless Communications and Sparse Sensing Radars in Clutter

Bo Li, *Student member, IEEE*, and Athina Petropulu, *Fellow, IEEE*

Abstract

The paper proposes a cooperative spectrum sharing scheme for a MIMO communication system and a matrix completion (MC) based, colocated MIMO (MIMO-MC) radar. MIMO-MC radars perform sub-Nyquist sampling at the receive antennas. To facilitate the co-existence, and also deal with clutter, both the radar and the communication systems use transmit precoding. For waveform flexibility, the radar uses a random unitary waveform matrix. We prove that for such waveforms and any precoding matrix, the error performance of matrix completion is guaranteed. The radar transmit precoder, the radar sub-sampling scheme, and the communication transmit covariance matrix are jointly designed in order to maximize the radar SINR, while meeting certain communication rate and power constraints. The joint design is implemented at a control center, which is a node with whom both systems share physical layer information, and which also performs data fusion for the radar. We also provide efficient optimization algorithms for the proposed optimization problem, along with insight on the feasibility and properties of the proposed design. Simulation results show that the proposed scheme significantly improves the spectrum sharing performance in various scenarios.

Index Terms

MIMO radar, matrix completion, spectrum sharing, precoding, alternating optimization, co-existence

I. Introduction

Traditionally, communication and radar systems use the radio spectrum in an exclusive fashion. However, recent studies have shown that large chunks of spectrum designated for radar applications are underutilized [1], while there is spectrum congestion in commercial wireless communications. Recently, there has been interest in enabling radar and communication system to operate in the same frequency band, so that both can make more efficient use of spectrum [2], [3]. Currently, high UHF radar systems overlap with GSM communication systems, and S-band radars partially overlap with Long Term Evolution (LTE) and WiMax systems [4]–[7]. The main problem with such

This work was supported by NSF under Grant ECCS-1408437.

Authors addresses: B. Li, A. P. Petropulu, Dept. of Electrical and Computer Engineering, Rutgers, the State University of New Jersey, 94 Brett Road, Piscataway, NJ 08854. E-mail: (athinap@rutgers.edu).

overlap is the interference that one system exerts to the other, which can be significant even for low levels of the interfering signal. According to [8], levels of interference to noise ratio below the thermal noise floor level of the radar receiver can reduce the probability of target detection. Also, the interference generated by the radar reduces the throughput of a communication system operating nearby. Spectrum sharing methods target at enabling radar and communication systems to share the spectrum efficiently by minimizing interference effects. The literature on spectrum sharing can be classified into three main classes. Works in the first class explore large physical separation distances [5], [6], [9] to control interference. Works in the second class explore dynamic spectrum access [10]–[14] by using OFDM signals and optimally allocating subcarriers [15]–[17], or synthesize radar waveforms in the frequency domain with controlled interference to the spectrally overlayed wireless communication systems [18]–[21]. However, these works do not explore the spatial degree of freedom that would greatly reduce the mutual interference. This of course would require multiple antennas at both systems. Works in the third class exploit multiple antennas at both the radar and the communication system, in order to enable radar and communication systems to co-exist on the same frequency band [7], [22]–[27], thus improving spectral efficiency as compared to the other two classes. Since our proposed method falls in this category, we will discuss this class in more detail.

Most of the existing multiple-input-multiple-output (MIMO) radar-communication spectrum sharing literature addresses interference mitigation either for the communication system [7], [22]–[24], or for the radar [27]. Spectrum sharing between MIMO radars and communication systems was initially considered in [7], [22]–[26], where the radar interference to the communication system was eliminated by projecting the radar waveforms onto the null space of the interference channel. However, projection-type techniques might miss targets lying in the row space of the interference channel. In addition, the interference generated by the communication system to the radar was not considered in [7], [22]–[26]. Spatial filtering at the radar receiver was proposed in [27] to reduce interference. In the above literature, spatial multiplexing has been applied to each system in isolation, missing out on potential performance improvements from a coordinated operation of the two systems. Recent advances in cognitive radio and cloud technology, provide a framework via which different systems achieve improved performance by coordinating their operation.

To the best of our knowledge, co-design of radar and communication systems for spectrum sharing was first proposed in [28]–[32]. Compared to the design of [7], [22]–[27], joint design has the potential to improve the spectrum utilization due to increased number of design degrees of freedom. Co-design requires access to physical layer information on both systems. For example, both systems would have to share physical layer information with a node designated as the *control center*, which would optimally design the signaling schemes of each system. Obviously, this requires a certain degree of cooperation, but the payback would be less less interference for the radar and higher throughput for the communication system. The amount of information that can be shared and the privacy issues involved would have to be evaluated in each case. Examples of radar systems that could be amenable to such cooperation include radar for autonomous vehicles, weather monitoring, etc.

This paper investigates spectrum sharing of a MIMO communication system and a matrix completion (MC) based, collocated MIMO radar (MIMO-MC) system [33]–[35]. Traditional MIMO radars transmit different waveforms from

their transmit (TX) antennas, and their receive (RX) antennas forward their measurements to a fusion center for further processing. At the fusion center, based on the measurements the "data matrix" is formulated, which contains all the information about the targets. For a relatively small number of targets, the data matrix is low-rank [33], thus it to be reconstructed with provably accuracy (under certain conditions) based on a small set of its entries, which may be corrupted by a small amount of noise [34], [36]. This observation is the basis of MIMO-MC radars; the RX antennas forward to the fusion center a small number of pseudo-randomly sub-Nyquist sampled measurements, along with their sampling scheme, each RX antenna partially filling a row of the measurement matrix. The full data matrix, corresponding to Nyquist sampled data, is stably recovered via MC techniques, with reconstruction error proportional to the noise level, and can subsequently be used for target detection via standard array processing methods [33]. The sub-sampling at the antennas avoids the need for high rate analog-to-digital converters, and the reduced amount of samples translates into power and bandwidth savings in the antenna-fusion center link. MIMO-MC radars can achieve the high resolution of traditional MIMO radars with significantly fewer samples and reduced hardware complexity. Compared to compressive sensing (CS) based MIMO radars [37]–[39], which is another sample-reduction approach in the literature, MIMO-MC radars avoid basis mismatch problems, and by recovering all missing data via matrix completion do not suffer from signal-to-noise ratio (SNR) loss due to data subsampling. Our previous work [28], [29] showed that MIMO-MC is particularly well suited for spectrum sharing. This is because the sparse sampling modulates the interference channel to the communication system and increases its null space, thus giving the opportunity to the communication system to transmit along that null space and avoid interfering with the radar.

In the above context, in this paper we propose a new cooperative spectrum sharing scheme for MIMO-MC radars and MIMO communication systems by building on our previous results [28]–[32]. The proposed approach exploits precoding at the radar as well as the communication system antennas, in order to maximize the radar signal-to-interference-plus-noise ratio (SINR) while enabling the communication system to meet its operational objective. In addition to enabling coexistence, the precoding allows the mitigation of the effects of clutter. The radar task at hand is target tracking in clutter, i.e., the target parameters obtained from previous tracking cycles are available for the following tracking cycle to optimize the transmission for better SINR performance [40]. Thus, similar to transmit beamforming literature [41]–[43], some target parameters, e.g., the number and directions of the targets, are assumed known *a priori*. The main contributions of the proposed work are summarized as follows:

1) We prove the feasibility of transmit precoding for MIMO-MC radars using random unitary waveforms. In particular, we show that the coherence of the data matrix of a transmit precoding based MIMO-MC radar is upper bounded by a small constant (see Theorem 2), a key condition for the applicability of matrix completion. Furthermore, the derived bound is independent of the transmit precoder as long as the resulted data matrix has rank equal to the number of targets. This means that we can design the precoder for the purpose of transmit beamforming and interference suppression, without affecting the incoherence property of the data matrix, etc. Random unitary waveforms can be easily generated. Thus, to preserve security, the radar can change those

waveforms periodically without affecting the matrix completion performance.

2) We propose an architecture for the control center, which is a node with increased computational power and coordinates the cooperation. The control center integrates the operation of a fusion center for the radar, and is also responsible for collecting information from the radar and communication systems, computing the jointly optimal signal scheme for spectrum sharing, and distributing the optimal scheme to each system. The introduction of the control center reduces the network complexity, and promotes cooperation while maintaining the privacy of the two systems.
3) We formulate an optimization problem, to be solved at the control center; the objective function is the SINR at the radar, and the constraints are the communication system rate and the radar and communication system power. The radar SINR considers interference from the communication system and also clutter. The solution consists of the communication transmit covariance matrices, the radar precoding matrix, and the radar sub-sampling scheme. In order to formulate the problem, the control center requires channel state information (CSI), and target and clutter parameters. Since the control center integrates the radar fusion center functionality, the target angles obtained from the previous tracking cycle are naturally available. In practice, the clutter parameters can be estimated when the targets are absent [43]. The problem is solved via alternating optimization. Insight on the problem feasibility and the rank of the obtained radar precoding matrix is also provided.

To the best of our knowledge, the joint design of transmit precoders and the radar clutter mitigation have not been considered in MIMO radar and communication coexistence literature. The proposed joint design involves high computational complexity. However, the computation capability of control centers grows exponentially thanks to techniques such as cloud computing and specialized integrated circuits.

A. Relation to the literature

The proposed MIMO-MC radar with precoding extends the work in [33], [35], where there is no transmit precoding, and the radar waveforms are obtained as the solution of a computationally intensive optimization problem. In contrast, our proposed approach supports waveform agility and can handle clutter and interference. The proposed approach extends the work in [28] and [29], where no precoding is used, and the radar interference at the communication receiver is controlled via subtraction of an estimate of the interference. However, such approach might not work well when the radar power is high and can saturate the communication receiver. Further, due to the random phase offset between the radar transmitter and the communication receiver, following the subtraction there will always be residual interference, which can degrade the communication system performance. Joint transmit precoding for the coexistence of *traditional* MIMO radars and a MIMO communication system was first studied in [30]–[32]. Our work here exploits radar precoding for the problem studied in [30]–[32]. The effect of precoding on the conditions for matrix completion is not straightforward to determine. One of the contributions of this paper is to prove that the matrix completion performance can still be guaranteed when radar precoding is used.

TABLE I: Notations

$\mathcal{CN}(\mu, \mathbf{\Sigma})$	the circularly symmetric complex Gaussian distribution with mean μ and covariance matrix $\mathbf{\Sigma}$
$\lvert\cdot\rvert$, $\mathrm{Tr}(\cdot)$	matrix determinant & trace
$\mathbb{N}_L^+$	the set $\{1, \ldots, L\}$
δ_{ij}	the Kronecker delta
x^+	$\max(0, x)$
$\lfloor x \rfloor$	the largest integer smaller or equal to x
$\Re(\cdot)$	the real part of a complex variable
$\mathbf{A}^T, \mathbf{A}^H$	the transpose and Hermitian transpose of $\mathbf{A}$
$\otimes$	the Kronecker product
$\circ$	the Hadamard product
$\lVert\mathbf{A}\rVert$	the spectral norm of matrix $\mathbf{A}$, *i.e.*, the largest singular value
$\lVert\mathbf{A}\rVert_*$	the nuclear norm of matrix $\mathbf{A}$, *i.e.*, the sum of singular values
$\lVert\mathbf{A}\rVert_F$	the Frobenius norm of matrix $\mathbf{A}$, *i.e.*, $\sqrt{\mathrm{Tr}(\mathbf{A}^H\mathbf{A})}$
$\mathbf{A}_{\cdot m}$	the m-th column vector of $\mathbf{A}$
$\mathbf{A}_{m\cdot}$	the m-th row vector of $\mathbf{A}$.
$[\mathbf{A}]_{i,j}$	the (i, j)-th element of matrix $\mathbf{A}$
$\mathcal{R}(\mathbf{A})$	the range (column space) of matrix $\mathbf{A}$

B. Organization

The paper is organized as follows. Section II starts with the background on MIMO-MC radars. We then provide the incoherence property for the MIMO-MC radars using random unitary waveforms and nontrivial precoders. Section III introduces the signal model when the MIMO-MC radar and communication systems coexisted. The problem of MIMO communication sharing spectrum with MIMO-MC radar is studied in Sections IV. Numerical results and conclusions are provided in Sections V-VI.

Notation: The notation is summarized in Table I.

II. MIMO-MC Radar Revisited

A. Background on MIMO-MC Radar

Consider a collocated MIMO radar system with $M_{t,R}$ TX antennas and $M_{r,R}$ RX antennas arranged as uniform linear arrays (ULA) with inter-element spacing d_t and d_r, respectively. The radar is pulse based with pulse repetition interval T_{PRI} and carrier wavelength λ_c. The K far-field targets are with distinct angles $\{\theta_k\}$, target reflection coefficients $\{\beta_k\}$ and Doppler shifts $\{\nu_k\}$ and are assumed to fall in the same range bin. Following the clutter-free model of [33]–[35], the noisy data matrix at the fusion/control center can be formulated as

$$\mathbf{Y}_R = \mathbf{V}_r \mathbf{\Sigma} \mathbf{V}_t^T \mathbf{P} \mathbf{S} + \mathbf{W}_R, \tag{1}$$

where the m-th row of $\mathbf{Y}_R \in \mathbb{C}^{M_{r,R}\times L}$ contains the L fast-time raw samples forwarded by the m-th antenna [40]; $\mathbf{S} = [\mathbf{s}(1), \cdots, \mathbf{s}(L)]$, if the waveform matrix, with $\mathbf{s}(l) = [s_1(l), \cdots, s_{M_{t,R}}(l)]^T$ being the l-th snapshot across the transmit antennas; the transmit waveforms are assumed to be orthogonal, *i.e.*, it holds that $\mathbf{S}\mathbf{S}^H = \mathbf{I}_{M_{t,R}}$ [33]; $\mathbf{W}_R$ denotes additive noise; and $\mathbf{P} \in \mathbb{C}^{M_{t,R}\times M_{t,R}}$ denotes the transmit precoding matrix. $\mathbf{V}_t \triangleq [\mathbf{v}_t(\theta_1), \ldots, \mathbf{v}_t(\theta_K)]$ and $\mathbf{V}_r \triangleq [\mathbf{v}_r(\theta_1), \ldots, \mathbf{v}_r(\theta_K)]$ respectively denote the transmit and receive steering matrix and $\mathbf{v}_r(\theta) \in \mathbb{C}^{M_{r,R}}$ is the receive steering vector defined as

$$\mathbf{v}_r(\theta) \triangleq \left[e^{-j2\pi 0\vartheta^r}, \ldots, e^{-j2\pi(M_{r,R}-1)\vartheta^r}\right]^T, \tag{2}$$

where $\vartheta^r = d_r \sin(\theta)/\lambda_c$ denotes the spatial frequency w.r.t. the receive array. $\mathbf{v}_t(\theta) \in \mathbb{C}^{M_{t,R}}$ is the transmit steering vector and is respectively defined. Matrix $\mathbf{\Sigma}$ is defined as $\mathbf{\Sigma} \triangleq \text{diag}([\beta_1 e^{j2\pi\nu_1}, \ldots, \beta_K e^{j2\pi\nu_K}])$. $\mathbf{D} \triangleq \mathbf{V}_r\mathbf{\Sigma}\mathbf{V}_t^T$ is the target response matrix. At the fusion center, $\mathbf{Y}_R$ passes through the matched filters, after which target estimation is performed via standard array processing methods [44].

When K is smaller than $M_{r,R}$ and L, the noise-free data matrix $\mathbf{M} \triangleq \mathbf{DPS}$ is low-rank and can be provably recovered based on a subset of its entries. This observation gave rise to MIMO-MC radars [33]–[35], where each RX antenna sub-samples the target returns and forwards the samples to the fusion center. The partially filled data matrix at the fusion center can be mathematically expressed as follows (see [33] Scheme I)

$$\mathbf{\Omega} \circ \mathbf{Y}_R = \mathbf{\Omega} \circ (\mathbf{M} + \mathbf{W}_R), \tag{3}$$

where $\circ$ denotes the Hadamard product; $\mathbf{\Omega}$ is the sub-sampling matrix containing 0's and 1's. The sub-sampling rate p equals $\|\mathbf{\Omega}\|_0/(LM_{r,R})$. When $p = 1$, the $\mathbf{\Omega}$ matrix is filled with 1's, and the MIMO-MC radar is identical to the traditional MIMO radar. At the fusion center, the completion of $\mathbf{M}$ can be achieved by the following nuclear norm minimization problem [36]

$$\min_{\mathbf{M}} \|\mathbf{M}\|_* \quad \text{s.t. } \|\mathbf{\Omega} \circ \mathbf{M} - \mathbf{\Omega} \circ \mathbf{Y}_R\|_F \leq \delta, \tag{4}$$

where $\delta > 0$ is a parameter determined by the sampled entries of the noise matrix, *i.e.*, $\mathbf{\Omega} \circ \mathbf{W}_R$. It is shown in [36] that the recovery of $\mathbf{M}$ is stable against noise. The matrix recovery error is proportional to the noise level δ, given that the following conditions hold [36]

- $\mathbf{M}$ is incoherent with parameters (μ_0, μ_1),
- $\mathbf{\Omega}$ corresponds to uniformly at random sub-sampling operation with $m \triangleq M_{r,R}Lp \geq CKn\log n$, where $n \triangleq \max\{M_{r,R}, L\}$.

It is important to note that, under the above conditions, the noise free data matrix, $\mathbf{M}$, can be stably reconstructed with high accuracy, thus preserving all the received target echo power. The incoherence parameters (μ_0, μ_1) are given by $\mu_0 \geq \max(\mu(U), \mu(V))$, $\mu_1\sqrt{\frac{K}{M_{r,R}L}} \geq \|\sum_{k=1}^K \mathbf{U}_{\cdot k}\mathbf{V}_{\cdot k}^H\|_\infty$, where $\mathbf{U} \in \mathbb{C}^{M_{r,R}\times K}$ and $\mathbf{V} \in \mathbb{C}^{L\times K}$ contain the left and right singular vectors of $\mathbf{M}$; the coherence of subspace V spanned by basis matrix $\mathbf{V}$ is defined as

$$\mu(V) \triangleq \frac{L}{K}\max_{1\leq l\leq L}\|\mathbf{V}_{l\cdot}\|^2 \in \left[1, \frac{L}{K}\right].$$

In [35], upper bounds on the incoherence parameters of $\mathbf{M}$ were derived for the case $\mathbf{P} = \mathbf{I}$. Those bounds, along

with the orthogonality property of the radar waveforms were used to design waveforms with good incoherence properties (see Theorem 2 of [35]). The work of [35] involves numerical optimization on the complex Stiefel manifold, which has high computational complexity. However, radar waveforms need to be updated frequently as security against adversaries, which makes the issue of computational cost more severe.

It was shown in [33] that the matrix completion performance degrades severely when the SINR drops below 10 dB [33], which suggests that along with "good" radar waveforms, a precoder design for interference mitigation is very important. In the following, we consider radar precoder design in order to maximize the radar SINR, and propose to use a random unitary matrix [45] as the waveform matrix $\mathbf{S}$. This choice of waveform matrix is motivated by the simulations in [35] which show that the random unitary matrix performs almost the same as the optimally designed waveform. While the effect of such waveform matrix on matrix completion was studied in [35], the effect of the precoder as well as the waveform matrix on matrix completion is analyzed in the following subsection. We should note that the results of [35] cannot be easily extended for a nontrivial transmit precoding case.

B. MIMO-MC Radar Using Random Unitary Matrix

A random unitary matrix [45] can be obtained through Gram-Schmidt orthogonalization of a random matrix with entries distributed as i.i.d Gaussian. This means that we can generate waveform candidates easily. The following theorem provides an upper bound on the incoherence parameter $\mu(V)$ of $\mathbf{M}$ when random unitary waveform is used and a non-trivial radar precoder $\mathbf{P}$ is employed.

Theorem 1. *(Bounding $\mu(V)$) Consider the MIMO-MC radar presented in Section II-A with $\mathbf{S}$ being random unitary. For any transmit precoder $\mathbf{P}$ such that the rank of $\mathbf{M}$ is $K_0 \leq K$, and arbitrary transmit array geometry and target angles, the coherence of subspace V obeys the following:*

$$\mu(V) \leq \frac{K_0 + 2\sqrt{3K_0 \ln L} + 6 \ln L}{K_0} \triangleq \tilde{\mu}_0^t$$

with probability $1 - L^{-2}$.

Proof: The proof can be found in Appendix A. ■

The proof uses algebraic manipulations and the non-asymptotic probability bounds on Gaussian random vectors [46]. Based on Theorem 1, we have the following theorem for the incoherence parameters of $\mathbf{M}$.

Theorem 2. *(Coherence of $\mathbf{M}$ with random unitary waveform matrix) Consider the MIMO-MC radar presented in Section II-A with $\mathbf{S}$ being random unitary. On denoting the Fejér kernel by $F_n(x)$, for $d_r = \lambda_c/2$, arbitrary transmit array geometry, and*

$$K \leq \sqrt{M_{r,R}/F_{M_{r,R}}(\xi_r)},$$

the matrix $\mathbf{M}$ is incoherent with parameters $\mu_0 \triangleq \max\{\frac{K}{K_0}\mu_0^r, \tilde{\mu}_0^t\}$ and $\mu_1 \triangleq \sqrt{K_0}\mu_0$ with probability $1 - L^{-2}$, where $\tilde{\mu}_0^t$ is defined in Theorem 1. μ_0^r is the upper bound on $\mu(U)$ derived in [35, Theorem 2]. The incoherence property of $\mathbf{M}$ holds for any precoding matrix $\mathbf{P}$ such that the rank of $\mathbf{M}$ is K_0.

Proof: The theorem can be proven by combining the bounds on $\mu(U)$ and $\mu(V)$ in [35, Theorem 2] and Theorem 1, respectively. ■

Remark 1. Some comments are in order. First, if K_0 is $\mathcal{O}(\ln L)$, the upper bound $\tilde{\mu}_0^t > 1$ is a small constant. Therefore, $\mathbf{M}$ has a good incoherent property. A similar bound was provided on the coherence of the subspaces spanned by random orthogonal basis in [47]. Second, unlike the results in [35, Theorem 2], the probabilistic bound on $\mu(V)$ is independent of the target angles and array geometry. Third, the above results hold for any random unitary matrix $\mathbf{S}$. The radar waveform can be changed periodically, which would be good for security reason, without affecting the matrix completion performance. Finally, the probabilistic bound on $\mu(V)$ in Theorem 1 is independent of $\mathbf{P}$. This means that we can design $\mathbf{P}$, without affecting the incoherence property of $\mathbf{M}$, for the purpose of transmit beamforming and interference suppression. This key observation validates the feasibility of radar precoding based spectrum sharing approaches for MIMO-MC radar and communication systems in the sequel. Note that this paper focuses on the design of radar precoder in the spatial domain, not the waveform. The radar precoder will not affect the waveform ambiguity property in the time and Doppler domains.

III. System Model and Problem Formulation

We consider the coexistence scenario in [29], as shown in Fig. 1, where a MIMO-MC radar system and a MIMO communication system operate using the same carrier frequency. Note that the coexistence model is general, because when full sampling is adopted the MIMO-MC radar turns to be a traditional MIMO radar. In the coexistence system, $\mathbf{H} \in \mathbb{C}^{M_{r,C} \times M_{t,C}}$ denotes the communication channel, where $M_{r,C}$ and $M_{t,C}$ denote respectively the number of RX and TX antennas of the communication system; $\mathbf{G}_1 \in \mathbb{C}^{M_{r,C} \times M_{t,R}}$ and $\mathbf{G}_2 \in \mathbb{C}^{M_{r,R} \times M_{t,C}}$ denote the interference channels between the communication and radar systems.

The cooperative spectrum sharing can be implemented via the system architecture of Fig. 2. The coordination of the cooperation is conducted by a control center, which collects information from the two systems, formulates and solves an optimization problem, and passes to each systems its optimal parameters. The control center can be thought of as an enhanced Spectrum Access System (SAS) used in the FCC release [48], and is connected to the radar/communication system via either a wireless link, or a backhaul channel.

The control center can also integrate the functionality of the radar fusion center, i.e., target detection, estimation and tracking, and specifically for the MIMO-MC radar considered in this paper, also matrix completion. There are several advantages in having a control center that encompasses the radar fusion center. First, a powerful all-in-one center greatly simplifies the complexity of the overall network. Second, radar operators, especially in military applications, are not willing to share information directly with civilian cellular systems out of security concerns. In such cases the control center can be operated by the radar, and enables cooperation while maintaining the isolation of the radar and communication systems. Third, the radar and communication systems only need communication interfaces with the control system.

In order to establish our coexistence model, the key assumptions made in this paper are summarized as follows.

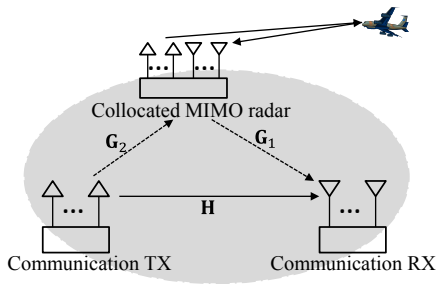

Fig. 1: A MIMO communication system sharing spectrum with a colocated MIMO radar system

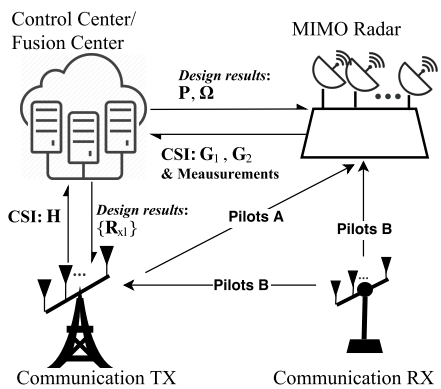

Fig. 2: The proposed spectrum sharing architecture. The cooperation is coordinated by the control center, a node with high computing power that also serves as the radar fusion center. The control center collects information from radar and communication systems, computes jointly optimal signaling schemes for both systems and sends each scheme back to the corresponding system.

a) Signal bandwidth: We assume that the two systems transmit narrowband waveforms with the same symbol period. To evaluate the feasibility of radar and communication systems having the same symbol period, let us consider an S-band search and acquisition radar with range resolution equal to $300m$ (a typical range resolution is between $100m$ and $600m$ [49], [50]). The corresponding radar sub-pulse duration is $2\mu s$. Communication symbol duration should of $2\mu s$, are quite typical in model cellular systems [51]. The transmitted signal is narrowband if the channel coherence bandwidth is larger than the signal bandwidth [51]–[53]. In a macro-cell, typical values for the channel coherence bandwidth are of the order of 1 MHz [54], [55], which is much larger than the signal bandwidth of 0.5 MHz (or symbol interval $2\mu s$). Thus, the narrowband assumption is typically valid. If higher signal bandwidth is needed, OFDM signaling can be used for both radar [15], [17] and the communication system [54], [55]. Our coexistence model can still be valid on each OFDM carrier, over which the signal can be considered as narrowband.

b) About fading: We assume that $\mathbf{H}$, $\mathbf{G}_1$ and $\mathbf{G}_2$ are flat fading, which is valid when the transmitted signals are narrowband. The flat fading assumption is a common practice in the radar-communication system coexistence literature [7], [22]–[25]. In addition, all channels are assumed to be block fading over the radar pulse repetition

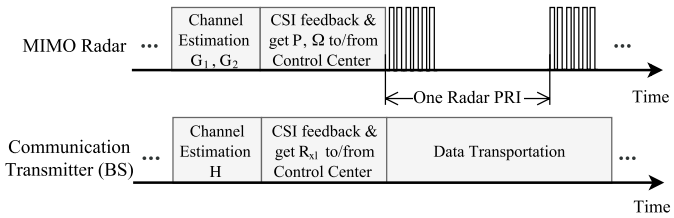

Fig. 3: TDM based CSI estimation and feedback and reception of design results from the control center.

interval (PRI). For a radar with medium pulse repetition frequency, the pulse repetition interval is usually between 30μs and 0.3 ms. The typical channel coherence time for 2.5 GHz and 5.8 GHz carrier frequency ranges from 2 ms up to 200 ms [56]. The channel coherence time is much larger than the radar pulse repetition interval. As for the moving targets, the resulting Doppler shifts are usually assumed to be constant during one PRI [40], [57]. Therefore, channel block fading is a reasonable assumption.

c) About CSI: The channel $\mathbf{H}$ is assumed to be perfectly known at the communication transmitter. The channels $\mathbf{G}_1$ and $\mathbf{G}_2$ are also assumed to be perfectly known at the radar. The CSI estimation can be achieved using pilot channels [7], [58] scheduled by the control center in FDM or TDM fashion. As a simple example, based on Fig. 2, the communication transmitter, i.e., the base station (BS), transmits a reference signal in pilot burst A, and this is used by the radar to estimate $\mathbf{G}_2$. The communication receiver, i.e., a user entity (UE), transmits a reference signal in pilot bursts B, and this is used by the BS and the radar to estimate $\mathbf{H}$ and $\mathbf{G_1}$, respectively, based on channel reciprocity [59]. All estimated CSI is sent to the control center by the radar and the BS, where it is used to jointly optimize the spatial multiplexing. Note that CSI estimation and feedback can be scheduled based on the channel coherence time, which is much larger than the radar pulse repetition interval. Figure 3 shows a simplified schematic diagram for CSI estimation/feedback and receiving design results from the control center based on TDM. Existing techniques in cognitive radios and multiuser MIMO (MU-MIMO) [60]–[66] can also be applied to reduce the overhead for CSI feedback.

d) About the radar mode of operation: We consider the target tracking scenario, in which the radar searches in particular directions of interest given by set $\{\theta_k\}$ and a range bin of interest for targets with unknown RCS variances [41], [42]. In such scenario, the target parameters have typically been obtained from previous tracking cycles, and are used to optimize the transmission for better SINR performance [40].

Under the above assumptions, let us consider the same target scene in a particular range bin as in Section II-A but with clutter. The baseband signal received by the radar and communication receivers during L symbol durations

in one radar pulse repetition interval can be expressed as

Radar receiver:

$$\mathbf{\Omega} \circ \mathbf{Y}_R = \mathbf{\Omega} \circ \big(\underbrace{\mathbf{DPS}}_{\text{signal}} + \underbrace{\mathbf{CPS} + \mathbf{G}_2\mathbf{X}\mathbf{\Lambda}_2}_{\text{interference}} + \underbrace{\mathbf{W}_R}_{\text{noise}}\big), \tag{5a}$$

Communication receiver:

$$\mathbf{Y}_C = \underbrace{\mathbf{HX}}_{\text{signal}} + \underbrace{\mathbf{G}_1\mathbf{PS}\mathbf{\Lambda}_1}_{\text{interference}} + \underbrace{\mathbf{W}_C}_{\text{noise}}, \tag{5b}$$

where $\mathbf{Y}_R$, $\mathbf{D}$, $\mathbf{P}$, $\mathbf{S}$, $\mathbf{W}_R$, and $\mathbf{\Omega}$ are defined in Section II-A. Note that delay in the radar signal model is assumed a prior in current tracking cycle and properly compensated. The waveform-dependent interference $\mathbf{CPS}$ contains interferences from point scatterers (clutter or interfering objects). Suppose that there are K_c point clutters with angles $\{\theta_k^c\}$, reflection coefficients $\{\beta_k^c\}$ in the same range bin as the targets. $\mathbf{C} \triangleq \sum_{k=1}^{K_c} \beta_k^c \mathbf{v}_r(\theta_k^c)\mathbf{v}_t^T(\theta_k^c)$ is the clutter response matrix. $\mathbf{Y}_C$ and $\mathbf{W}_C$ denote the received signal and additive noise at the communication RX antennas, respectively. The columns of $\mathbf{X} \triangleq [\mathbf{x}(1), \ldots, \mathbf{x}(L)]$ are codewords from the code-book of the communication system. We assume that $\mathbf{W}_{R/C}$ contains i.i.d random entries distributed as $\mathcal{CN}(0, \sigma_{R/C}^2)$. The diagonal matrix $\mathbf{\Lambda}_i, i \in \{1, 2\}$ contains the random phase offset $e^{j\alpha_{il}}$ between the MIMO-MC radar and the communication system at the l-th symbol. The time-varying phase offsets are results of the random phase jitters of the oscillators between the radar transmitter and the communication receiver and vice versa [29], [67]. Note that the Doppler shift will not be an issue for the proposed design in our paper. The radar signal model in (5a) is for the fast-time samples received in one radar pulse. In the radar literature, the Doppler shift is usually assumed to be constant during one radar pulse [38], [40], [57], [68]. Therefore, as shown in our signal model, the Doppler shift can be absorbed into the target RCS, and does not affect our proposed design.

The control center aims to protect the radar system and maximize the spectrum efficiency. In the following, we propose for the control center a joint design of the communication and radar transmissions, so that we minimize the interference at the radar RX antennas for successful matrix completion, while satisfying certain communication system requirements.

IV. The Proposed Spectrum Sharing Method

In this section, we first derive the communication rate and radar SINR in terms of communication and radar waveforms and formulate the MIMO-MC radar and MIMO communication spectrum sharing problem. In Section IV-A, an optimization algorithm is proposed using alternating optimization. Insight on the feasibility and properties of the proposed problem is provided in IV-B. We briefly discuss the spectrum sharing formulations for constant-rate communication transmission and traditional MIMO radars respectively in Section IV-C and IV-D.

For the communication system, the covariance of interference plus noise is given by

$$\mathbf{R}_{\text{Cin}} = \mathbf{G}_1\mathbf{\Phi}\mathbf{G}_1^H + \sigma_C^2\mathbf{I} \tag{6}$$

where $\mathbf{\Phi} \triangleq \mathbf{P}\mathbf{P}^H/L$ is positive semidefinite. For $l \in \mathbb{N}_L^+$, the *instaneous* information rate is unknown because the interference plus noise is not necessarily Gaussian due to the random phase offset $\alpha_1(l)$. Instead, we are interested

in a lower bound of the rate, which is given by [69]

$$\underline{C}(\mathbf{R}_{xl}, \mathbf{\Phi}) \triangleq \log_2 \left| \mathbf{I} + \mathbf{R}_{\text{Cin}}^{-1} \mathbf{H} \mathbf{R}_{xl} \mathbf{H}^H \right|,$$

which is achieved when the codeword $\mathbf{x}(l)$, $l \in \mathbb{N}_L^+$ is distributed as $\mathcal{CN}(0, \mathbf{R}_{xl})$. The average communication rate over L symbols is as follows

$$C_{\text{avg}}(\{\mathbf{R}_{xl}\}, \mathbf{\Phi}) \triangleq \frac{1}{L} \sum_{l=1}^{L} \underline{C}(\mathbf{R}_{xl}, \mathbf{\Phi}), \tag{7}$$

where $\{\mathbf{R}_{xl}\}$ denotes the set of all $\mathbf{R}_{xl}$'s.

The MIMO-MC radar only partially samples $\mathbf{Y}_R$. Therefore, only the sampled target signal and sampled interference determine the matrix completion performance. Based on this observation, we define the *effective signal power* (ESP) and *effective interference power* (EIP) at the radar RX node as follows

$$\begin{aligned} \text{ESP} &\triangleq \mathbb{E}\left\{ \text{Tr}\left(\mathbf{\Omega} \circ (\mathbf{DPS}) \left(\mathbf{\Omega} \circ (\mathbf{DPS})^H \right) \right) \right\} \\ &= pLM_{r,R} \text{Tr}\left(\mathbf{\Phi} \mathbf{D}_t \right), \end{aligned} \tag{8}$$

$$\text{EIP} \triangleq pLM_{r,R} \text{Tr}\left(\mathbf{\Phi} \mathbf{C}_t \right) + \sum\nolimits_{l=1}^{L} \text{Tr}\left(\mathbf{G}_{2l} \mathbf{R}_{xl} \mathbf{G}_{2l}^H \right), \tag{9}$$

where $\mathbf{D}_t = \sum_{k=1}^{K} \sigma_{\beta_k}^2 \mathbf{v}_t^*(\theta_k) \mathbf{v}_t^T(\theta_k)$, $\mathbf{C}_t = \sum_{k=1}^{K_c} \sigma_{\beta_k^c}^2 \mathbf{v}_t^*(\theta_k^c) \mathbf{v}_t^T(\theta_k^c)$, σ_{β_k} and $\sigma_{\beta_k^c}$ denote the standard deviation of β_k and β_k^c, respectively; $\mathbf{G}_{2l} \triangleq \mathbf{\Delta}_l \mathbf{G}_2$ and $\mathbf{\Delta}_l = \text{diag}(\mathbf{\Omega}_{\cdot l})$. The derivation can be found in Appendix B, which assumes that each of the target and clutter reflection coefficient is an independent complex Gaussian variable with zero mean, which is widely considered in the literature [42], [43], [70].

Remark 2. The sub-sampling at the radar receiver effectively modulates the interference channel $\mathbf{G}_2$ from the communication transmitter to the radar receiver. At sampling time l, only the interferences at radar RX antennas corresponding to 1's in $\mathbf{\Omega}_{\cdot l}$ are sampled. Equivalently, the effective interference channel during the l-th symbol duration is $\mathbf{G}_{2l}$. Therefore, adaptive communication transmission with symbol dependent covariance matrix $\mathbf{R}_{xl}$ is used in order to match the variation of the effective interference channel $\mathbf{G}_{2l}$ [29]. The disadvantage is high computational cost. A sub-optimal alternative is constant rate communication transmission, *i.e.*, $\mathbf{R}_{xl} \equiv \mathbf{R}_x, \forall l \in \mathbb{N}_L^+$, outlined in Section IV-C. □

Incorporating the expressions for effective target signal, interference and additive noise, the *effective* radar SINR is given as

$$\text{ESINR} = \frac{\text{Tr}\left(\mathbf{\Phi} \mathbf{D}_t \right)}{\text{Tr}\left(\mathbf{\Phi} \mathbf{C}_t \right) + \sum_{l=1}^{L} \text{Tr}\left(\mathbf{G}_{2l} \mathbf{R}_{xl} \mathbf{G}_{2l}^H \right) / (pLM_{r,R}) + \sigma_R^2}.$$

One can see that the joint design of the communication TX covariance matrices $\{\mathbf{R}_{xl}\}$, the radar precoder $\mathbf{P}$ (embedded in $\mathbf{\Phi}$), and the radar sub-sampling scheme $\mathbf{\Omega}$ is necessary to maximize the ESINR. In Theorem 2, we prove that the radar precoder $\mathbf{P}$ can be designed without affecting the incoherence property of $\mathbf{M}$. At the control

center, the spectrum sharing problem can be formulated as follows

$$(\mathbf{P}_1) \quad \max_{\{\mathbf{R}_{xl}\}\succeq 0, \mathbf{\Phi}\succeq 0, \mathbf{\Omega}} \text{ESINR}\left(\{\mathbf{R}_x\}, \mathbf{\Omega}, \mathbf{\Phi}\right),$$

$$\text{s.t. } C_{\text{avg}}(\{\mathbf{R}_{xl}\}, \mathbf{\Phi}) \geq C, \tag{10a}$$

$$\sum_{l=1}^{L} \text{Tr}\left(\mathbf{R}_{xl}\right) \leq P_C, L\text{Tr}\left(\mathbf{\Phi}\right) \leq P_R, \tag{10b}$$

$$\text{Tr}\left(\mathbf{\Phi}\mathbf{V}_k\right) \geq \xi \text{Tr}(\mathbf{\Phi}), \forall k \in \mathbb{N}_K^+, \tag{10c}$$

$$\mathbf{\Omega} \text{ is proper}, \tag{10d}$$

where $\mathbf{V}_k \triangleq \mathbf{v}_t^*(\theta_k)\mathbf{v}_t^T(\theta_k)$. The constraint of (10a) restricts the communication rate to be at least C, in order to support reliable communication and avoid service outage. The constraints of (10b) restrict the total communication and radar transmit power to be no larger than P_C and P_R, respectively. The constraints of (10c) restrict that the power of the radar probing signal at interested directions must be not smaller than that achieved by the uniform precoding matrix $\frac{\text{Tr}(\mathbf{\Phi})}{M_{t,R}}\mathbf{I}$, *i.e.*, $\mathbf{v}_t^T(\theta_k)\mathbf{\Phi}\mathbf{v}_t^*(\theta_k) \geq \xi \mathbf{v}_t^T(\theta_k)\frac{\text{Tr}(\mathbf{\Phi})}{M_{t,R}}\mathbf{I}\mathbf{v}_t^*(\theta_k) = \xi \text{Tr}(\mathbf{\Phi})$. $\xi \geq 1$ is a parameter used to control the beampattern at the interested target angles. The purpose of this constraint is to ensure fairness across the multiple targets. The constraint in (10d) imposes the restrictions on the radar sub-sampling matrix $\mathbf{\Omega}$ such that it corresponds to a fixed sub-sampling rate p and has large spectral gap[1] [71].

In order for the control center to formulate and solve the problem of (10) it needs (i) the communication and radar system CSI; estimation and feedback of CSI is discussed in Section III. (ii) target angles, and clutter parameters $\{\sigma_{\beta_k^c}^2\}$ and $\{\theta_k^c\}$. Since the control center integrates the radar fusion center functionality, the target angles obtained from the previous tracking cycle will be available. In practice, the clutter parameters could be estimated when the targets are absent [43]. If $\{\sigma_{\beta_k}^2\}$ is not known, we can instead use a single value σ_0^2 for all the targets. This choice effectively means that the objective treats all target directions equally. One possible choice for σ_0^2 is the smallest target RCS variance that could be detected by the radar. Note that the solution of $(\mathbf{P}_1)$ is independent on the specific value of σ_0^2. (iii) all parameters in the constraints. Parameters like power budget and required communication rate can also be provided by the radar and communication systems.

Problem $(\mathbf{P}_1)$ is non-convex w.r.t. optimization variable triple $(\{\mathbf{R}_x\}, \mathbf{\Omega}, \mathbf{\Phi})$. We propose an algorithm to find a local solution via alternating optimization in Subsection IV-A. In Subsection IV-B, we provide some insights on the feasibility and solution properties for $(\mathbf{P}_1)$.

A. Solution to $(\mathbf{P}_1)$ *Using Alternating Optimization*

The alternating iterations w.r.t. $\{\mathbf{R}_{xl}\}$, $\mathbf{\Omega}$, and $\mathbf{\Phi}$ are discussed in the following three subsections.

[1]In matrix completion literature, $\mathbf{\Omega}$ is either a uniformly random sub-sampling matrix [36], or the adjacency matrix of a regular bipartite graph with large spectral gap [71]. The spectral gap of a matrix is defined as the difference between the largest singular value and the second largest singular value.

1) **The Alternating Iteration w.r.t. $\{\mathbf{R}_{xl}\}$:** We first solve for $\{\mathbf{R}_{xl}\}$ while setting $\mathbf{\Omega}$ and $\mathbf{\Phi}$ to be equal to the solution from the previous iteration:

$$\begin{aligned}(\mathbf{P_R}) \quad & \min_{\{\mathbf{R}_{xl}\}\succeq 0} \sum_{l=1}^{L} \mathrm{Tr}\left(\mathbf{G}_{2l}\mathbf{R}_{xl}\mathbf{G}_{2l}^H\right) \\ & \text{s.t. } C_{\text{avg}}(\{\mathbf{R}_{xl}\},\mathbf{\Phi}) \geq C, \sum_{l=1}^{L} \mathrm{Tr}\left(\mathbf{R}_{xl}\right) \leq P_C.\end{aligned} \tag{11}$$

Problem $(\mathbf{P_R})$ is convex and involves multiple matrix variables, the joint optimization with respect to which requires high computational complexity. The semidefinite matrix variables $\{\mathbf{R}_{xl}\}$ have $LM_{t,C}^2$ real scalar variables, which will results in a complexity of $\mathcal{O}((LM_{t,C}^2)^{3.5})$ if an interior-point method [72] is used. An efficient algorithm for solving the above problem can be implemented based on the Lagrangian dual decomposition [72]. Please refer to [29, Algorithm 1] for the detailed solution. The complexity of the dual decomposition based algorithm is only linearly dependent on L.

2) **The Alternating Iteration w.r.t. $\mathbf{\Omega}$:** By simple algebraic manipulation, the EIP from the communication transmission can be reformulated as

$$\sum_{l=1}^{L} \mathrm{Tr}\left(\mathbf{G}_{2l}\mathbf{R}_{xl}\mathbf{G}_{2l}^H\right) \equiv \mathrm{Tr}(\mathbf{\Omega}^T\mathbf{Q}),$$

where the l-th column of $\mathbf{Q}$ contains the diagonal entries of $\mathbf{G}_2\mathbf{R}_{xl}\mathbf{G}_2^H$. With fixed $\{\mathbf{R}_{xl}\}$ and $\mathbf{\Phi}$, we can solve $\mathbf{\Omega}$ via

$$\min_{\mathbf{\Omega}} \ \mathrm{Tr}(\mathbf{\Omega}^T\mathbf{Q}) \quad \text{s.t. } \mathbf{\Omega} \text{ is proper}, \tag{12}$$

Recall that the sampling matrix $\mathbf{\Omega}$ is required to have large spectral gap. However, it is difficult to incorporate such conditions in the above optimization problem. Based on the fact that row and column permutation of the sampling matrix would not affect its singular values and thus the spectral gap, our prior work [29] proposed a suboptimal approach to search the best sampling scheme by permuting rows and columns of an initial sampling matrix $\mathbf{\Omega}^0$, *i.e.*,

$$\min_{\mathbf{\Omega}} \ \mathrm{Tr}(\mathbf{\Omega}^T\mathbf{Q}) \quad \text{s.t. } \mathbf{\Omega} \in \wp(\mathbf{\Omega}^0), \tag{13}$$

where $\wp(\mathbf{\Omega}^0)$ denotes the set of matrices obtained by arbitrary row and/or column permutations. $\mathbf{\Omega}^0$ is generated with binary entries and $\lfloor pLM_{r,R}\rfloor$ ones. Therefore, the constraint on number of 1's in $\mathbf{\Omega}$ can also be satisfied. One good candidate for $\mathbf{\Omega}^0$ would be a uniformly random sampling matrix, as such matrix exhibits large spectral gap with high probability [71]. Multiple trials with different $\mathbf{\Omega}^0$'s can be used to further improve the choice of $\mathbf{\Omega}$. However, the search space is very large since $|\wp(\mathbf{\Omega}^0)| = \Theta(M_{r,R}!L!)$. In this paper, we propose to reduce the search space as follows

$$\min_{\mathbf{\Omega}} \ \mathrm{Tr}(\mathbf{\Omega}^T\mathbf{Q}) \equiv \mathrm{Tr}(\mathbf{\Omega}\mathbf{Q}^T) \quad \text{s.t. } \mathbf{\Omega} \in \wp_r(\mathbf{\Omega}^0), \tag{14}$$

where $\wp_r(\mathbf{\Omega}^0)$ denotes the set of matrices obtained by arbitrary row permutations. The search space in (14) $|\wp_r(\mathbf{\Omega}^0)| = \Theta(M_{r,R}!)$ is greatly reduced compared to that in (13). Furthermore, the following proposition shows that such reduction of search space comes without any performance loss.

$$\mathbf{A}_l \triangleq -\left(\frac{\partial \underline{C}(\mathbf{R}_{xl},\mathbf{\Phi})}{\partial \Re(\mathbf{\Phi})}\right)^T_{\mathbf{\Phi}=\bar{\mathbf{\Phi}}} = \mathbf{G}_1^H[(\mathbf{G}_1\mathbf{\Phi}\mathbf{G}_1^H+\sigma_C^2\mathbf{I})^{-1}-(\mathbf{G}_1\mathbf{\Phi}\mathbf{G}_1^H+\sigma_C^2\mathbf{I}+\mathbf{H}\mathbf{R}_{xl}\mathbf{H}^H)^{-1}]\mathbf{G}_1\big|_{\mathbf{\Phi}=\bar{\mathbf{\Phi}}}. \quad (15)$$

Proposition 1. *For any $\mathbf{\Omega}^0$, searching for an $\mathbf{\Omega}$ in $\wp_r(\mathbf{\Omega}^0)$ can achieve the same EIP as searching in $\wp(\mathbf{\Omega}^0)$.*

Proof: We can prove the proposition by showing that the EIP achieved by any $\mathbf{\Omega}_1 \in \wp(\mathbf{\Omega}^0)$ can also be achieved by a certain $\mathbf{\Omega}_2 \in \wp_r(\mathbf{\Omega}^0)$. For the pair $(\mathbf{\Omega}_1, \{\mathbf{R}_{xl}\})$, the same EIP can be achieved by the pair $(\mathbf{\Omega}_2, \{\tilde{\mathbf{R}}_{xl}\})$, where

- $\mathbf{\Omega}_2$ is constructed by performing on $\mathbf{\Omega}^0$ the row permutations performed from $\mathbf{\Omega}^0$ to $\mathbf{\Omega}_1$, and
- $\{\tilde{\mathbf{R}}_{xl}\}$ is a permutation of $\{\mathbf{R}_{xl}\}$ according to the column permutations performed from $\mathbf{\Omega}^0$ to $\mathbf{\Omega}_1$.

In other words, the column permutations on $\mathbf{\Omega}$ is unnecessary because $\{\mathbf{R}_{xl}\}$ will be automatically optimized to match the column pattern of $\mathbf{\Omega}$. The claim is proven. ■

The problem in (14) aims to find the best one-to-one match between the rows of $\mathbf{\Omega}^0$ and the rows of $\mathbf{Q}$. Let us construct a cost matrix $\mathbf{C}^r \in \mathbb{R}^{M_{r,R}\times M_{r,R}}$ with $[\mathbf{C}^r]_{ml} \triangleq \mathbf{\Omega}^0_{m\cdot}(\mathbf{Q}_{l\cdot})^T$. The problem turns out to be a linear assignment problem with cost matrix $\mathbf{C}^c$, which can be solved efficiently in polynomial time $\mathcal{O}(M_{r,R}^3)$ using the Hungarian algorithm [73].

3) **The Alternating Iteration w.r.t. $\mathbf{\Phi}$***:* For the optimization of $\mathbf{\Phi}$ with fixed $\{\mathbf{R}_{xl}\}$ and $\mathbf{\Omega}$, the constraint in (10a) is nonconvex w.r.t. $\mathbf{\Phi}$. The first order Taylor expansion of $\underline{C}(\mathbf{R}_{xl},\mathbf{\Phi})$ at $\bar{\mathbf{\Phi}}$ is given as

$$\underline{C}(\mathbf{R}_{xl},\mathbf{\Phi}) \approx \underline{C}(\mathbf{R}_{xl},\bar{\mathbf{\Phi}}) - \mathrm{Tr}\left[\mathbf{A}_l(\mathbf{\Phi}-\bar{\mathbf{\Phi}})\right],$$

where $\mathbf{A}_l$ is given in (15) on the top of next page.

The sequential convex programming technique is applied to solve $\mathbf{\Phi}$ by repeatedly solve the following approximate optimization problem

$$\begin{aligned}(\mathbf{P}_{\mathbf{\Phi}})\ \max_{\mathbf{\Phi}\succeq 0}\ & \frac{\mathrm{Tr}(\mathbf{\Phi}\mathbf{D}_t)}{\mathrm{Tr}(\mathbf{\Phi}\mathbf{C}_t)+\rho},\\ \text{s.t.}\ & \mathrm{Tr}\left(\mathbf{\Phi}\right) \le P_R/L, \mathrm{Tr}\left(\mathbf{\Phi}\mathbf{A}\right) \le \tilde{C},\\ & \mathrm{Tr}\left(\mathbf{\Phi}\mathbf{V}_k\right) \ge \xi \mathrm{Tr}\left(\mathbf{\Phi}\right), \forall k \in \mathbb{N}_K^+,\end{aligned} \quad (16)$$

where $\tilde{C} = \sum_{l=1}^L(\underline{C}(\mathbf{R}_{xl},\bar{\mathbf{\Phi}})+\mathrm{Tr}(\bar{\mathbf{\Phi}}\mathbf{A}_l)-C)$, $\mathbf{A} = \sum_{l=1}^L \mathbf{A}_l$, $\rho = \sum_{l=1}^L \mathrm{Tr}\left(\mathbf{R}_{xl}\mathbf{G}_2^H\mathbf{\Delta}_l\mathbf{G}_2\right)/(pLM_{r,R})+\sigma_R^2$ are real positive constants w.r.t. $\mathbf{\Phi}$, and $\bar{\mathbf{\Phi}}$ is updated as the solution of the previous repeated problem. Problem (16) could be equivalently formulated as a semidefinite programming problem (SDP) via Charnes-Cooper Transformation [43], [74].

$$\begin{aligned}\max_{\tilde{\mathbf{\Phi}}\succeq 0,\phi>0}\ & \mathrm{Tr}(\tilde{\mathbf{\Phi}}\mathbf{D}_t),\\ \text{s.t.}\ & \mathrm{Tr}(\tilde{\mathbf{\Phi}}\mathbf{C}_t) = 1-\phi\rho\\ & \mathrm{Tr}\left(\tilde{\mathbf{\Phi}}\right) \le \phi P_R/L, \mathrm{Tr}\left(\tilde{\mathbf{\Phi}}\mathbf{A}\right) \le \phi\tilde{C},\\ & \mathrm{Tr}\left(\tilde{\mathbf{\Phi}}(\mathbf{V}_k-\xi\mathbf{I})\right) \ge 0, \forall k \in \mathbb{N}_K^+.\end{aligned} \quad (17)$$

The optimal solution of (17), denoted by $(\tilde{\mathbf{\Phi}}^*, \phi^*)$, can be obtained by using any standard interior-point method based SDP solver with a complexity of $\mathcal{O}((M_{t,R}^2)^{3.5})$. The solution of (16) is given by $\tilde{\mathbf{\Phi}}^*/\phi^*$. In each alternating iteration w.r.t. $\mathbf{\Phi}$, it is required to solve several iterations of SDP due to the sequential convex programming.

It is easy to show that the objective function, *i.e.*, ESINR, is nondecreasing during the alternating iterations of $\{\mathbf{R}_{xl}\}$, $\mathbf{\Omega}$ and $\mathbf{\Phi}$, and is upper bounded. According to the monotone convergence theorem [75], the alternating optimization is guaranteed to converge. The proposed efficient spectrum sharing algorithm in presence of clutter using a lower bound of the radar SINR is summarized in Algorithm 1.

Algorithm 1 Spectrum sharing algorithm for $(\mathbf{P}_1)$.

Input: $\mathbf{D}_t, \mathbf{C}_t, \mathbf{H}, \mathbf{G}_1, \mathbf{G}_2, P_{C/R}, C, \sigma_{C/R}^2, \delta_1$
Initialization: $\mathbf{\Phi} = \frac{P_R}{LM_{t,R}}\mathbf{I}$, $\mathbf{\Omega} = \mathbf{\Omega}^0$;
repeat
  Update $\{\mathbf{R}_{xl}\}$ by solving $(\mathbf{P_R})$ with fixed $\mathbf{\Omega}$ and $\mathbf{\Phi}$;
  Update $\mathbf{\Omega}$ by solving (14) with fixed $\{\mathbf{R}_{xl}\}$ and $\mathbf{\Phi}$;
  Update $\mathbf{\Phi}$ by solving a sequence of approximated SDP problem (16) with fixed $\{\mathbf{R}_{xl}\}$ and $\mathbf{\Omega}$;
until ESINR increases by amount smaller than δ_1
Output: $\{\mathbf{R}_{xl}\}, \mathbf{\Omega}, \mathbf{P} = \sqrt{L}\mathbf{\Phi}^{1/2}$

B. Insights on the Feasibility and Solutions of $(\mathbf{P}_1)$

In this subsection, we provide some key insights on the feasibility of $(\mathbf{P}_1)$ and the rank of the solutions $\mathbf{\Phi}$ obtained by Algorithm 1.

1) **Feasibility***:* A necessary condition on C for the feasibility of $(\mathbf{P}_1)$ w.r.t. $\{\mathbf{R}_{xl}\}$ is $C \leq C_{\max}(P_C)$ where

$$C_{\max}(P_C) \triangleq \max_{\{\mathbf{R}_{xl}\}\succeq 0} \frac{1}{L}\sum_{l=1}^{L} \log_2 \left|\mathbf{I} + \sigma_C^{-2}\mathbf{H}\mathbf{R}_{xl}\mathbf{H}^H\right|,$$
$$\text{s.t.} \sum_{l=1}^{L} \mathrm{Tr}\left(\mathbf{R}_{xl}\right) \leq P_C$$

The above optimization problem is convex and has a closed-form solution based on water-filling [52]. It can be shown that $C_{\max}(P_C)$ is essentially the largest achievable communication rate when there is no interference from radar transmitters to the communication receivers. Note that $C = C_{\max}(P_C)$ will generate a nonempty feasible set for $\{\mathbf{R}_{xl}\}$ only if $\mathbf{G}_1\mathbf{\Phi}\mathbf{G}_1^H = \mathbf{0}$, *i.e.*, the radar transmits in the null space of the interference channel $\mathbf{G}_1$ to the communication receivers[2].

A necessary condition on ξ for the feasibility of $(\mathbf{P}_1)$ w.r.t. $\mathbf{\Phi}$ is $\xi \leq \xi_{\max}$ where

$$\xi_{\max} \triangleq \max_{\mathbf{\Phi}\succeq 0, \xi\geq 0} \xi, \text{ s.t. } \mathrm{Tr}(\mathbf{\Phi}\mathbf{V}_k) \geq \xi \mathrm{Tr}(\mathbf{\Phi}), \forall k \in \mathbb{N}_K^+.$$

[2]We omit the trivial case $\mathbf{\Phi} = \mathbf{0}$.

Note that the above optimization problem is independent of $\text{Tr}(\mathbf{\Phi})$. Without loss of generality, we assume that $\text{Tr}(\mathbf{\Phi}) = 1$, based on which we have the following equivalent SDP formulation

$$\xi_{\text{max}} \triangleq \max_{\mathbf{\Phi}\succeq 0, \xi \geq 0} \xi, \text{ s.t. } \text{Tr}(\mathbf{\Phi}) = 1,$$
$$\text{Tr}(\mathbf{\Phi}\mathbf{V}_k) \geq \xi, \forall k \in \mathbb{N}_K^+.$$

It is easy to check that $\xi_{\text{max}} \geq 1$, which can be achieved by set $(\mathbf{\Phi}, \xi)$ to be $(\mathbf{I}/M_{t,R}, 1)$.

The following proposition provides a sufficient condition for the feasibility of $(\mathbf{P}_1)$.

Proposition 2. *If $C, \xi, P_C > 0, P_R > 0$ are chosen such that $C < C_{max}(P_C)$ and $\xi \leq \xi_{max}$, then $(\mathbf{P}_1)$ is feasible.*

Proof: The proof can be found in Appendix C. ■

2) **The Rank of the Solutions $\mathbf{\Phi}$***:* We are also particularly interested in the rank of $\mathbf{\Phi}$ obtained using Algorithm 1. Since the sequential convex programming technique is used for solving $\mathbf{\Phi}$, it suffices to focus on the rank of the solution of $(\mathbf{P}_{\mathbf{\Phi}})$. To achieve this goal, we first introduce the following SDP problem

$$\begin{aligned} &\min_{\mathbf{\Phi}\succeq 0} \text{Tr}\left(\mathbf{\Phi}\right) \text{ s.t. } \text{Tr}\left(\mathbf{\Phi}\mathbf{A}\right) \leq \tilde{C}, \ \frac{\text{Tr}(\mathbf{\Phi}\mathbf{D}_t)}{\text{Tr}(\mathbf{\Phi}\mathbf{C}_t) + \rho} \geq \gamma, \\ &\text{Tr}\left(\mathbf{\Phi}\mathbf{V}_k\right) \geq 0, \forall k \in \mathbb{N}_K^+. \end{aligned} \tag{18}$$

where γ is a real positive constant. The following proposition relates the optimal solutions of problems (16) and (18).

Proposition 3. *If γ in (18) is chosen to be the maximum achievable SINR of (16), denoted as $SINR_{max}$, the optimal $\mathbf{\Phi}$ of (18) is also optimal for (16).*

Proof: Denote $\mathbf{\Phi}_1^*$ and $\mathbf{\Phi}_2^*$ the optimal solutions of (16) and (18), respectively. It is clear that $\mathbf{\Phi}_1^*$ is feasible point of (18). This means that $\text{Tr}(\mathbf{\Phi}_2^*) \leq \text{Tr}(\mathbf{\Phi}_1^*) \leq P_R$. Therefore, $\mathbf{\Phi}_2^*$ is a feasible point of (16). It holds that

$$\text{SINR}_{\text{max}} \equiv \frac{\text{Tr}(\mathbf{\Phi}_1^*\mathbf{D}_t)}{\text{Tr}(\mathbf{\Phi}_1^*\mathbf{C}_t) + \rho} \geq \frac{\text{Tr}(\mathbf{\Phi}_2^*\mathbf{D}_t)}{\text{Tr}(\mathbf{\Phi}_2^*\mathbf{C}_t) + \rho} \geq \text{SINR}_{\text{max}}.$$

It is only possible when all the equalities hold. In other words, $\mathbf{\Phi}_2^*$ is optimal for (16). The claim is proved. Note that SINR_{max} is introduced as an intermediate for the proof. ■

In order to characterize the optimal solution of (18), we need the following key lemma:

Lemma 1. *Matrix $\mathbf{A}_l$ defined in (15) and thus $\mathbf{A}$ are positive semidefinite.*

Proof: The proof can be found in Appendix D. ■

Based on Lemma 1, we prove the following result by following the approach in [74]:

Proposition 4. *Suppose that (18) is feasible when γ is set to $SINR_{max}$. Then, any optimal solution of (18) has rank at most K. All rank-K solutions $\mathbf{\Phi}_K^*$ of (18) have the same range space. Any solution $\mathbf{\Phi}_{K^-}^*$ with rank less than K has range space such that $\mathcal{R}(\mathbf{\Phi}_{K^-}^*) \subset \mathcal{R}(\mathbf{\Phi}_K^*)$. Moreover, (16) and (17) always have solutions with rank at most K and with the same range space properties as that for (18).*

Proof: The proof can be found in Appendix E. ■

The proof is based on the Karush-Kuhn-Tucker (KKT) conditions [72]. Proposition 4 indicates that the rank of the optimal precoding matrix will not be larger than the number of the targets.

C. Constant-Rate Communication Transmission

The adaptive communication transmission in the proposed spectrum sharing methods involves high complexity. A sub-optimal transmission approach of constant rate, *i.e.*, $\mathbf{R}_{xl} \equiv \mathbf{R}_x, \forall l \in \mathbb{N}_L^+$, has a lower implementation complexity. In such case, the spectrum sharing problem can be reformulated as

$$\begin{aligned}(\mathbf{P}_1') \quad & \max_{\mathbf{R}_x \succeq 0, \mathbf{\Phi} \succeq 0} \text{ESINR}'(\mathbf{R}_x, \mathbf{\Omega}, \mathbf{\Phi}), \\ & \text{s.t. } \underline{C}(\mathbf{R}_x, \mathbf{\Phi}) \geq C, \\ & \quad L\text{Tr}\left(\mathbf{R}_x\right) \leq P_C, L\text{Tr}\left(\mathbf{\Phi}\right) \leq P_R, \\ & \quad \text{Tr}\left(\mathbf{\Phi}\mathbf{V}_k\right) \geq 0, \forall k \in \mathbb{N}_K^+,\end{aligned}$$

where

$$\text{ESINR}' = \frac{\text{Tr}\left(\mathbf{\Phi}\mathbf{D}_t\right)}{\text{Tr}\left(\mathbf{\Phi}\mathbf{C}_t\right) + \text{Tr}\left(\mathbf{\Delta}\mathbf{G}_2\mathbf{R}_x\mathbf{G}_2^H\right)/(pLM_{r,R}) + \sigma_R^2}$$

and $\mathbf{\Delta} = \sum_{l=1}^{L} \mathbf{\Delta}_l$ is diagonal and with each entry equal to the number of 1's in the corresponding row of $\mathbf{\Omega}$. Similar techniques in Algorithm 1 can be used to solve $(\mathbf{P}_1')$.

We can see that $(\mathbf{P}_1')$ has much lower complexity because there is only one matrix variable for the communication transmission. However, the drawback of the constant-rate communication is that $\mathbf{R}_x$ cannot adapt to the variation of the effective interference channel $\mathbf{G}_{2l}$. On the other hand, the adaptive communication transmission considered in $(\mathbf{P}_1)$ can fully exploit the channel diversity introduced by the radar sub-sampling procedure. It will be seen in the simulations of Section V-C, the constant-rate transmission from the solution of (19) is inferior to the adaptive transmission from the solution of (10).

Another consequence is that the ESINR$'$ depends on $\mathbf{\Omega}$ only through $\mathbf{\Delta}$. Since $\mathbf{\Omega}$ is searched among the row permutations of a uniformly random sampling matrix, the number of 1's in each row of $\mathbf{\Omega}$ is close to pL, or equivalently, $\mathbf{\Delta}$ will be very close to the scaled identity matrix $pL\mathbf{I}$. To further reduce the complexity, the optimization w.r.t. $\mathbf{\Omega}$ in $(\mathbf{P}_1')$ is omitted because all row permutations of $\mathbf{\Omega}$ will result in a very similar ESINR$'$. From a different perspective, if the radar sub-sampling matrix $\mathbf{\Omega}$ is not available for the radar and communication cooperation, we can safely replace $\mathbf{\Delta}$ with $pL\mathbf{I}$ in the ESINR$'$. The above discussion asserts that, for the case of constant-rate communication transmission almost no performance degradation occurs due to the absence of the knowledge of $\mathbf{\Omega}$.

D. Traditional MIMO Radars

The traditional MIMO radars without sub-sampling can be considered as special case with $p = 1$, and thus there is no need for the matrix completion. In such case, the constant-rate communication transmission becomes optimal

scheme because the interference channel $\mathbf{G}_2$ stays as a constant for the period of L symbol time due to the block fading assumption. The spectrum sharing problem has the same form as $(\mathbf{P}_1')$ with the objective function being

$$\text{SINR} = \frac{\text{Tr}\left(\mathbf{\Phi}\mathbf{D}_t\right)}{\text{Tr}\left(\mathbf{\Phi}\mathbf{C}_t\right) + \text{Tr}\left(\mathbf{G}_2\mathbf{R}_x\mathbf{G}_2^H\right)/M_{r,R} + \sigma_R^2}.$$

Note that SINR $\approx$ ESINR$'$ because $\mathbf{\Delta} \approx pL\mathbf{I}$. Therefore, traditional MIMO radars can achieve approximately the same spectrum sharing performance as MIMO-MC radars when the communication system transmits at a constant rate. However, for MIMO-MC radars, the adaptive communication transmission and the radar sub-sampling matrix can be designed to achieve significant radar SINR increase over the traditional MIMO radars. This advantageous flexibility is introduced by the sparse sensing (*i.e.* sub-sampling) in MIMO-MC radars.

V. Numerical Results

In this section, we provide simulation examples to quantify the performance of the proposed spectrum sharing method for the coexistence of the MIMO-MC radars and communication systems.

Unless otherwise stated, we use the following default values for the system parameters. The MIMO radar system consists of collocated $M_{t,R} = 16$ TX and $M_{r,R} = 16$ RX antennas, respectively forming transmit and receive half-wavelength uniform linear arrays. The radar waveforms are chosen from the rows of a random orthonormal matrix [28]. We set the length of the radar waveforms to $L = 16$. The wireless communication system consists of collocated $M_{t,C} = 4$ TX and $M_{r,C} = 4$ RX antennas, respectively forming transmit and receive half-wavelength uniform linear arrays. For the communication capacity and power constraints, we take $C = 16$ bits/symbol and $P_C = 6400$ (the power is normalized by the additive noise power). The radar transmit power budget is $P_R = 1000 \times P_C$, which is typical for radar systems; high power is needed to to combat path loss associated with far-field targets [40]. The additive white Gaussian noise variances are $\sigma_C^2 = \sigma_R^2 = 1$. There are three stationary targets with RCS variance $\sigma_{\beta 0}^2 = 0.5$, located in the far-field with pathloss 10^{-3}. Clutter is generated by four point scatterers, all having the same RCS variance, σ_β^2; the variance is determined by the clutter to noise ratio (CNR) $10\log\sigma_\beta^2/\sigma_R^2$. Based on these numbers, the possible range of SNR at the communication receiver is between 12 dB and 26 dB, which is supported by LTE systems [76], [77]. The radar power budget corresponds to a per receive antenna SNR of about 23 dB when only additive noise is considered. For a typical radar system with a single antenna, operating with probability of detection of 0.9 and probability of false alarm of 10^{-6}, the required SNR is about 13.2 dB [40]. However, the actual SNR may be much smaller because spatial degrees of freedom are used to mitigate clutter and interference from the communication systems.

The channel $\mathbf{H}$ is modeled as Rayleigh fading, *i.e.*, contains independent entries, distributed as $\mathcal{CN}(0,1)$. The interference channels $\mathbf{G}_1$ and $\mathbf{G}_2$ are modeled as Rician fading. The power in the direct path is 0.1, and the variance of Gaussian components contributed by the scattered paths is 10^{-3}.

The performance metrics considered in this paper include the following:

- The radar *effective* SINR, *i.e.*, the objective of the spectrum sharing problem;
- The matrix completion relative recovery error, defined as $\|\mathbf{M} - \hat{\mathbf{M}}\|_F / \|\mathbf{M}\|_F$, where $\hat{\mathbf{M}}$ is the completed data matrix at the radar fusion center;

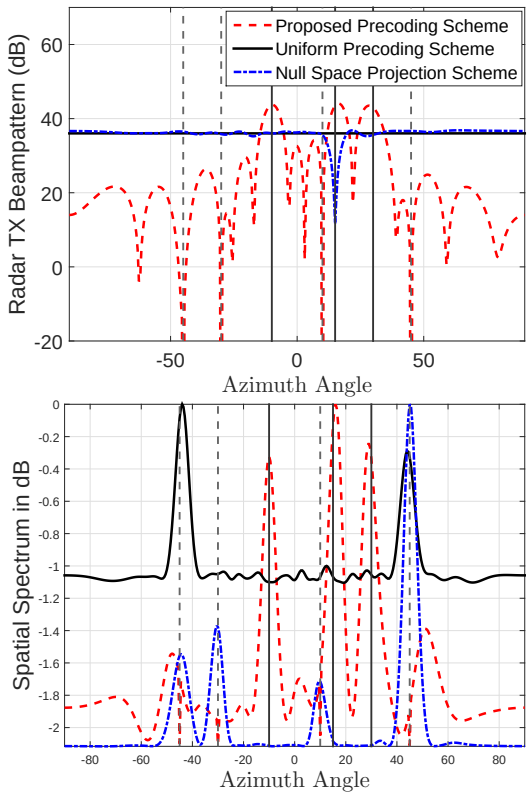

Fig. 4: The radar transmit beampattern and the MUSIC spatial pseudo-spectrum for MIMO-MC radar and communication spectrum sharing. $M_{t,R} = M_{r,R} = 16, M_{t,C} = M_{r,C} = 4$. The true positions of the targets and clutters are labeled using solid and dashed vertical lines, respectively. CNR=30 dB.

- The radar transmit beampattern, *i.e.*, the transmit power for different azimuth angles $\mathbf{v}_t^T(\theta)\mathbf{P}\mathbf{v}_t^*(\theta)$;
- The MUSIC pseudo-spectrum and the relative target RCS estimation RMSE obtained using the least squares estimation on the completed data matrix $\hat{\mathbf{M}}$.

Monte Carlo simulations with 100 independent trials are carried out to get an average performance.

A. The Radar Transmit Beampattern and MUSIC Spectrum

In this subsection, we present an example to show the advantages of the proposed radar precoding scheme as compared to the trivial uniform precoding, *i.e.*, $\mathbf{P} = \sqrt{LP_R/M_{t,R}}\mathbf{I}$, and null space projection (NSP) precoding, *i.e.*, $\mathbf{P} = \sqrt{LP_R/M_{t,R}}\mathbf{V}\mathbf{V}^H$, where $\mathbf{V}$ contains the basis of the null space of $\mathbf{G}_1$ [24]. For the proposed joint-design based scheme in (10), we choose $\xi = \lfloor \xi_{\max} \rfloor$. The target angles w.r.t. the array are respectively $-10°$, $15°$, and $30°$; the four point scatterers are at angles $-45°$, $-30°$, $10°$, and $45°$. The CNR is 30 dB. In this simulation, the direct path in $\mathbf{G}_1$ is generated as $\sqrt{0.1}\mathbf{v}_t(\phi)\mathbf{v}_t^H(\phi)$, where $\phi = 15°$, with $\mathbf{v}_t(\phi)$ is defined in (2). In other words, the communication receiver is taken at the same azimuth angle as the second target.

Recall that the NSP technique projects the radar waveform onto the null space of the interference channel $\mathbf{G}_2$

Precoding schemes	ESINR	MC Relative Recovery Errors	Relative RCS Est. RMSE
Joint-design precoding	31.3dB	0.038	0.028
Uniform precoding	-44.3dB	1.00	1.000
NSP based precoding	-46.3dB	1.00	0.995

TABLE II: The radar ESINR, MC relative recovery errors, and the relative target RCS estimation RMSE for MIMO-MC radar and communication spectrum sharing. The simulation setting is the same as that for Fig. 4.

in order to avoid creating interference to the communication receiver. Because the null space and row space of a matrix are orthogonal to each other, there will be no radar power radiated along the null space of $\mathbf{G}_2$, thus, targets in those locations will be missed. Our proposed approach does not suffered from such scenario, because the precoding is computed via the proposed joint design method instead of projecting to the null space of $\mathbf{G}_2$. The radar transmit beampattern and the spatial pseudo-spectrum obtained using the MUSIC algorithm are shown in Fig. 4. The correspondingly achieved ESINR, MC relative recovery error, and relative target RCS estimation RMSE are listed in Table II. We observe that the proposed joint-design based precoding scheme achieves significant improvement in ESINR, MC relative recovery error, and target RCS estimation accuracy. As expected, the uniform precoding scheme just spreads the transmit power uniformly in all directions. The NSP precoding scheme achieves a similar beampattern as the uniform precoding scheme, with the exception of the deep null that the NSP places in the direction of the communication receiver. The null means that the transmit power towards the second target is severely attenuated and thus the probability of missing the second target is increased. Neither the uniform nor the NSP precoding schemes have any capability of clutter mitigation. From Fig. 4, we observe that the proposed joint-design based precoding scheme successfully focuses the transmit power towards the three targets and nullifies the power towards the point scatterers. The three targets can be accurately estimated from the pseudo-spectrum obtained by the proposed scheme. Meanwhile, the communication system can still achieve the required rate by aligning its transmission along a channel subspace that does not interfere with the radar emissions. This unique advantage is enabled by the proposed joint design of radar and communication transmissions.

B. Comparison of Different Levels of Cooperation

In this subsection, we compare several algorithms with different levels of radar and communication cooperation. The compared algorithms include

- Uniform radar precoding and selfish communication: the radar transmit antennas use the trivial precoding, *i.e.*, $\mathbf{P} = \sqrt{LP_R/M_{t,R}}\mathbf{I}$; and the communication system minimizes the transmit power to achieve certain average capacity without any concern about the interference it exerts to the radar system. This algorithm involves no radar and communication cooperation.
- NSP based radar precoding and selfish communication: the radar transmit antennas use the fixed precoding, *i.e.*, $\mathbf{P} = \sqrt{LP_R/M_{t,R}}\mathbf{V}\mathbf{V}^H$, while the selfish communication scheme is the same with the previous case.

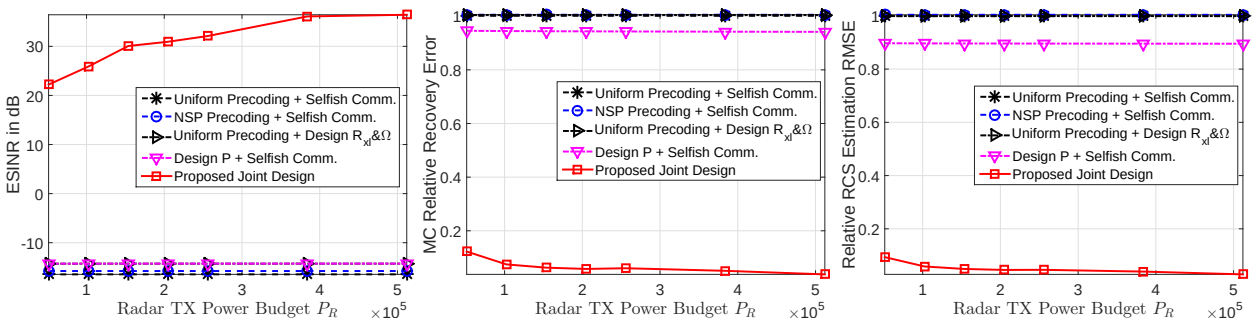

Fig. 5: Comparison of spectrum sharing with different levels of cooperation between the MIMO-MC radar and the communication system under different P_R. $M_{t,R} = M_{r,R} = 16, M_{t,C} = M_{r,C} = 4$.

- Uniform radar precoding and designing $\mathbf{R}_{xl}$ & $\mathbf{\Omega}$: only $\mathbf{R}_{xl}$ & $\mathbf{\Omega}$ are jointly designed to minimize the effective interference the radar receiver.
- Designing $\mathbf{P}$ and selfish communication: only the radar precoding matrix $\mathbf{P}$ is designed to maximize the radar ESINR.
- The proposed joint-design of $\mathbf{P}$, $\mathbf{R}_{xl}$, and $\mathbf{\Omega}$ in (10).

We use the same values for all parameters as in the previous simulation except that the radar transmit power budget P_R changes from $51,200$ to 2.56×10^6. Fig. 5 shows the achieved ESINR, the MC relative recovery error, and the relative target RCS estimation RMSE. The algorithms that use trivial uniform and NSP based radar precoding perform bad because the point scatterers are not properly mitigated. The scheme designing $\mathbf{P}$ only could mitigate the scatterers but the interference from the communication transmission is not controlled. The proposed joint design of $\mathbf{P}$, $\mathbf{R}_{xl}$, and $\mathbf{\Omega}$ simultaneously addresses the clutter and the mutual interference between the radar and the communication systems, and thus achieves the best performance amongst all the algorithms. The performance gains come from high level cooperation between the two systems.

C. Adaptive and Constant-rate Communication Transmissions

In this subsection, we evaluate the performance of two communication transmission schemes, namely, adaptive transmission with different $\mathbf{R}_{xl}$'s for all $l \in \mathbb{N}_L^+$, and constant-rate transmission with only one identical $\mathbf{R}_x$. We use the following parameter setting: $M_{t,R} = 16, M_{r,R} = M_{t,C} = 8, M_{r,C} = 2$, $C = 10$ bits/symbol, $P_C = 64$ and $P_R = 1000 \times P_C$. For the $\mathbf{G}_1$ and $\mathbf{G}_2$, Rayleigh fading is used with fixed $\sigma_{G_1}^2$ and varying $\sigma_{G_2}^2$. The results of ESINR, MC relative recovery error and the relative target RCS estimation RMSE for different values of $\sigma_{G_2}^2$ are shown in Fig. 6. The value of $\sigma_{G_2}^2$ varies from 0.05 to 0.5, which effectively simulates different distances between the communication transmitter and the radar receiver. It is clear that the adaptive communication transmission outperforms the constant-rate counterpart under various values of interference channel strength. As discussed in Section IV-C, the adaptive communication transmission can fully exploit the channel diversity of $\mathbf{G}_{2l}$ introduced by the radar sub-sampling procedure. The price for the performance advantages is high complexity. The average

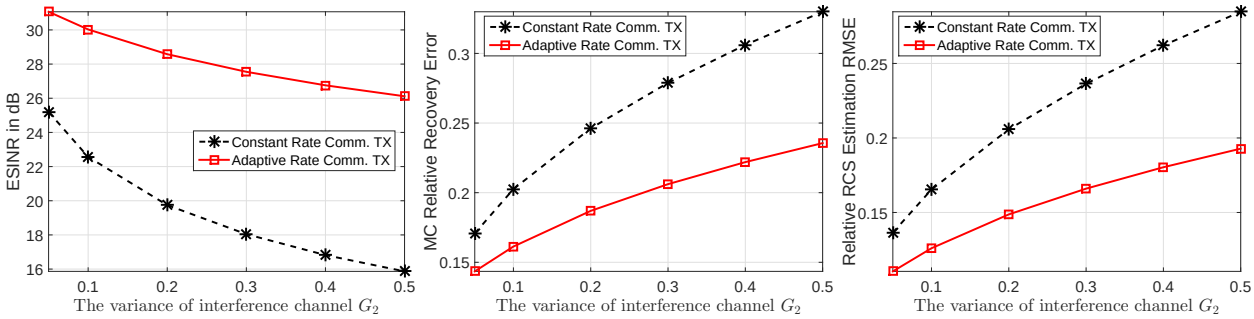

Fig. 6: Comparison of spectrum sharing with adaptive and constant-rate communication transmissions under different levels of variance of the interference channel from the communication transmitter to the radar receiver. $M_{t,R} = 16, M_{r,R} = M_{t,C} = 8, M_{r,C} = 2$.

running times for the adaptive and constant-rate communication transmissions are respectively 15.6 and 4.8 seconds. The choice between these two transmission schemes can be made depending on the available computing resources.

D. MIMO-MC Radars and Traditional MIMO Radars

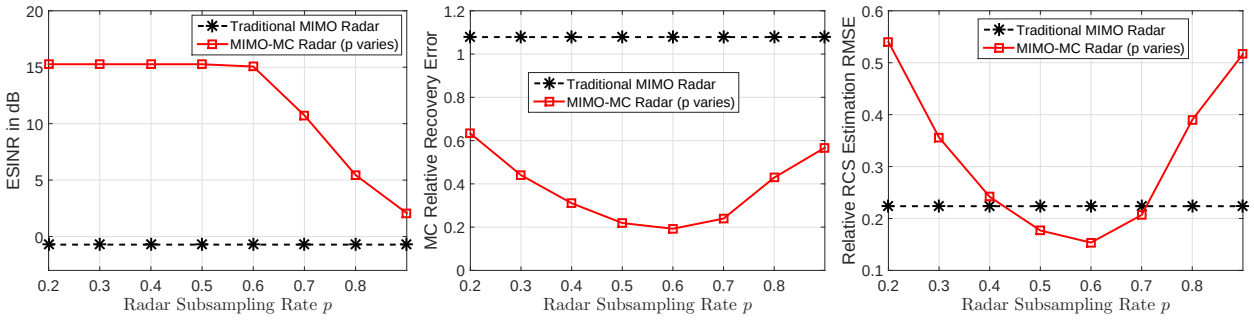

Fig. 7: Comparison of spectrum sharing with traditional MIMO radars and MIMO-MC radars with different subsampling rates p. $M_{t,R} = 16, M_{r,R} = M_{t,C} = 8, M_{r,C} = 2$.

In this subsection, we present a simulation to show the advantages of MIMO-MC radars compared to the traditional full-sampled MIMO radars. The parameters are the same as those in the previous simulation but with fixed $\sigma^2_{G_1} = 0.3$ and $\sigma^2_{G_2} = 1$, which indicates strong mutual interference, especially the interference from the communication transmitter to the radar receiver. The radar transmit power budget P_R is taken to be equal to $10 \times P_C$. We consider two targets; one is randomly located and the other is taken to be $25°$ away. We also consider 4 randomly located point scatterers. Fig. 7 shows the results under different MIMO-MC sub-sampling rates p. Note that full sampling is used for the traditional MIMO radar. The MC relative recover error for the traditional radar is actually the output distortion to signal ratio. A smaller distortion to signal ratio corresponds to a larger output SNR. For ease of comparison, a black dashed line is used for the traditional MIMO radar. We observe that the MIMO-MC radar achieves better performance in ESINR than the traditional radar. This is due to the fact that the communication

system can effectively prevent its transmission from interfering the radar system when the number of actively sampled radar RX antennas is small, *i.e.*, sub-sampling is small. In addition, the larger ESINR of the MIMO-MC radar results in a larger output SNR than that of the traditional radar. Furthermore, the MIMO-MC radar achieves better target RCS estimation accuracy than the traditional radar if its sub-sampling rate is between 0.4 and 0.7. For p larger than 0.7, the target RCS estimation accuracy achieved by the MIMO-MC radar is worse than that achieved by the traditional radar because small ESINRs for $p \geq 0.7$ introduce high distortion in the completed data matrix. The results in Fig. 7 could be used to help the selection of radar sub-sampling rate p. For the best target RCS estimation accuracy, $p = 0.6$ is the best choice, while for the biggest savings in terms of samples and similar performance as traditional radars, $p = 0.4$ is the best choice. Since there is no closed form solution for the joint design problem, it is difficult to provide a theoretical justification. Intuitively, the explanation of why $p = 0.6$ achieves the best MC recovery error and RCS estimation RMSE is the following. As p gets smaller, the matrix completion is not as accurate because there are fewer sample available. On the other hand, as p increases, the performance gets worse because more noisy samples are used in the matrix completion (smaller ESINR). Therefore, it seems that there is an optimum value of p, which in this case is $p = 0.6$.

Based on these results, we conclude that MIMO-MC radars can coexist with communication systems and achieve better target RCS estimation than traditional radars while saving up to 60% data samples. Such significant advantage is introduced by the sparse sensing (*i.e.* sub-sampling) in MIMO-MC radars as discussed in Section IV-D.

VI. Conclusions

In this paper, we have considered the co-existence of a MIMO-MC radar and a wireless MIMO communication system by sharing a common carrier frequency. We prove the feasibility of transmit precoding for MIMO-MC radars using random unitary waveforms. The radar transmit precoder, the radar sub-sampling scheme, and the communication transmit covariance matrix have been jointly designed by the control center to maximize the radar SINR while meeting certain rate and power constraints for the communication system. Random unitary waveforms can be easily generated and updated for waveform security. We should note that the proposed joint design based spectrum sharing method can also be applied to traditional MIMO radars, which is a special case of MIMO-MC radars for $p = 1$.

The proposed joint design based spectrum sharing algorithm has been evaluated via extensive simulations. Specifically, we have shown the superiority introduced by radar and communication cooperation in the proposed algorithm compared to noncooperative counterparts. The proposed joint-design based spectrum sharing scheme successfully focuses the transmit power towards the targets and nullifies the power towards the clutter. The proposed method achieves significant improvement in ESINR, MC relative recovery error, and target RCS estimation accuracy. We have also compared the performance and complexity of the adaptive and the constant-rate communication transmission schemes for radar-communication spectrum sharing. Finally, we have provided simulation-based comparison of MIMO-MC radars and traditional MIMO radars co-existing with communication systems. We have observed that the MIMO-MC radar achieves better performance in terms of ESINR and output SNR. Our simulations suggest that

MIMO-MC radars can co-exist with communication systems and achieve better target RCS estimation than traditional radars, while saving up to 60% in data samples. Of course these advantages come at increased computations for matrix completion.

We should note that the constraint requiring that the number of targets is smaller than the number of radar antennas results in an inefficient usage of the MIMO radar degrees of freedom. However, the high resolution of traditional MIMO radar is retained by MIMO-MC radars with a great reduction of sample and hardware complexity. The considered signal model is for narrow-band waveforms. Broadband MIMO systems typically use OFDM waveforms [16]. In such case, our proposed design still applies on individual component carriers. This will substantially expand the application scenarios of the work in this paper. A thorough investigation will be considered in our future work.

APPENDIX A
PROOF OF THEOREM 1

Proof: The following proof extends the results in [34], [35] for the cases where the radar employs transmit precoder $\mathbf{P}$ and random unitary waveform matrix $\mathbf{S}$, *i.e.*, $\mathbf{M} = \mathbf{V}_r \mathbf{\Sigma} \mathbf{V}_t^T \mathbf{P} \mathbf{S}$. The following lemma is used.

Lemma 2 ([46]). *Let S_N be a χ^2 random variable with N degrees of freedom. Then for each $t > 0$*

$$Pr\left(S_N - N \geq t\sqrt{2N} + t^2\right) \leq e^{-t^2/2}.$$

Denoting the rank of $\mathbf{M}$ by K_0, it is clear that K_0 is not larger than K. Recall that $\mathbf{M}$ has a compact SVD given as

$$\mathbf{M} = \mathbf{U} \mathbf{\Gamma} \mathbf{V}^H$$

where $\mathbf{U} \in \mathbb{C}^{M_{r,R} \times K_0}$ and $\mathbf{V} \in \mathbb{C}^{L \times K_0}$ contain the left and right singular vectors of $\mathbf{M}$; $\mathbf{\Gamma} \in \mathbb{R}^{K_0 \times K_0}$ is diagonal containing the singular values. Consider the QR decomposition of $\mathbf{V}_r$ and $\mathbf{S}^T \mathbf{P}^T \mathbf{V}_t$:

$$\mathbf{V}_r = \mathbf{Q}_r \mathbf{R}_r,$$

$$\mathbf{S}^T \mathbf{P}^T \mathbf{V}_t = \mathbf{Q}_t \mathbf{R}_t,$$

where $\mathbf{Q}_r \in \mathbb{C}^{M_{r,R} \times K}$ and $\mathbf{Q}_t \in \mathbb{C}^{L \times K_0}$ are with orthonormal columns, $\mathbf{R}_r \in \mathbb{C}^{K \times K}$ is upper triangular, and $\mathbf{R}_t \in \mathbb{C}^{K_0 \times K}$ has an upper staircase form. The matrix $\mathbf{R}_r \mathbf{\Sigma} \mathbf{R}_t^T \in \mathbb{C}^{K \times K_0}$ is full column rank with a compact SVD given by $\mathbf{U}_1 \mathbf{\Gamma}_1 \mathbf{V}_1^H$, where $\mathbf{U}_1 \in \mathbb{C}^{K \times K_0}$, $\mathbf{V}_1 \in \mathbb{C}^{K_0 \times K_0}$, $\mathbf{U}_1^H \mathbf{U}_1 = \mathbf{V}_1^H \mathbf{V}_1 = \mathbf{I}_{K_0}$, and $\mathbf{\Gamma}_1$ is diagonal, containing the singular values of $\mathbf{R}_r \mathbf{\Sigma} \mathbf{R}_t^T$. Therefore, we have

$$\mathbf{M} = \mathbf{Q}_r \mathbf{U}_1 \mathbf{\Gamma}_1 \mathbf{V}_1^H \mathbf{Q}_t^T = \mathbf{Q}_r \mathbf{U}_1 \mathbf{\Gamma}_1 (\mathbf{Q}_t^* \mathbf{V}_1)^H,$$

which is a valid SVD of $\mathbf{M}$. The uniqueness of singular value of a matrix indicates that $\mathbf{\Gamma} \equiv \mathbf{\Gamma}_1$. Therefore, we can choose $\mathbf{U} = \mathbf{Q}_r \mathbf{U}_1$ and $\mathbf{V} = \mathbf{Q}_t^* \mathbf{V}_1$. We have

$$\begin{aligned} \mu(U) &= \frac{M_{r,R}}{K_0} \sup_{m \in \mathbb{N}_{M_{r,R}}^+} \|(\mathbf{Q}_r)_{m\cdot} \mathbf{U}_1\|_2^2 \\ &\leq \frac{M_{r,R}}{K_0} \sup_{m \in \mathbb{N}_{M_{r,R}}^+} \|(\mathbf{Q}_r)_{m\cdot}\|_2^2 = \frac{K}{K_0} \mu_0^r, \end{aligned} \tag{20}$$

where $\tilde{\mu}_0^t$ is defined in Theorem 1. μ_0^r is the upper bound on $\mu(U)$ derived in [35, Theorem 2]. We also have

$$\mu(V) = \frac{L}{K_0} \sup_{l \in \mathbb{N}_L^+} \|(\mathbf{Q}_t^*)_{l\cdot} \mathbf{V}_1\|_2^2 = \frac{L}{K_0} \sup_{l \in \mathbb{N}_L^+} \|(\mathbf{Q}_t)_{l\cdot}\|_2^2.$$

If K_0 is strictly smaller than K, we can not represent $\mathbf{Q}_t$ in terms of $\mathbf{S}^T\mathbf{P}^T\mathbf{V}_t$ and $\mathbf{R}_t$ because of the singularity of $\mathbf{R}_t$. To conquer this, we apply column permutations $\mathbf{F}$ on $\mathbf{R}_t$ to bring forward the first non-zero elements in each row $\mathbf{R}_t\mathbf{F} = \begin{pmatrix}\mathbf{R}_1 & \mathbf{R}_2\end{pmatrix}$ such that $\mathbf{R}_1 \in \mathbb{C}^{K_0 \times K_0}$ is square, upper triangular and invertible. The QR decomposition $\mathbf{S}^T\mathbf{P}^T\mathbf{V}_t$ can be re-written as

$$\mathbf{S}^T\mathbf{P}^T\mathbf{V}_t\mathbf{F} = \mathbf{Q}_t\begin{pmatrix}\mathbf{R}_1 & \mathbf{R}_2\end{pmatrix}.$$

We can represent $\mathbf{Q}_t$ as

$$\mathbf{Q}_t = \mathbf{S}^T\mathbf{P}^T\mathbf{V}_t\mathbf{F}_{K_0}\mathbf{R}_1^{-1},$$

where $\mathbf{F}_{K_0}$ denotes the first K_0 columns of $\mathbf{F}$. Substituting $\mathbf{Q}_t$ into $\mu(V)$, we obtain

$$\begin{aligned}\mu(V) &= \frac{L}{K_0} \sup_{l \in \mathbb{N}_L^+} \|\left(\mathbf{S}^T\right)_{l\cdot} \mathbf{P}^T\mathbf{V}_t\mathbf{F}_{K_0}\mathbf{R}_1^{-1}\|_2^2 \\ &= \frac{L}{K_0} \sup_{l \in \mathbb{N}_L^+} \left(\mathbf{S}^T\right)_{l\cdot} \mathbf{P}^T\mathbf{V}_t\mathbf{F}_{K_0}\mathbf{R}_1^{-1}\left(\mathbf{R}_1^{-1}\right)^H \mathbf{F}_{K_0}^H\mathbf{V}_t^H\mathbf{P}^*\left(\mathbf{S}^*\right)_{\cdot l}\end{aligned} \tag{21}$$

We can show that

$$\begin{aligned}\mathbf{R}_1^{-1}\left(\mathbf{R}_1^{-1}\right)^H &= \left(\mathbf{R}_1^H\mathbf{R}_1\right)^{-1} = \left(\mathbf{R}_1^H\mathbf{Q}_t^H\mathbf{Q}_t\mathbf{R}_1\right)^{-1} \\ &= \left(\mathbf{F}_{K_0}^H\mathbf{V}_t^H\mathbf{P}^*\mathbf{S}^*\mathbf{S}^T\mathbf{P}^T\mathbf{V}_t\mathbf{F}_{K_0}\right)^{-1} \\ &= \left(\mathbf{F}_{K_0}^H\mathbf{V}_t^H\mathbf{P}^*\mathbf{P}^T\mathbf{V}_t\mathbf{F}_{K_0}\right)^{-1}\end{aligned} \tag{22}$$

where the last equality holds because $\mathbf{S}\mathbf{S}^H = \mathbf{I}_{M_{t,R}}$. Consider the QR decomposition of $\mathbf{P}^T\mathbf{V}_t\mathbf{F}_{K_0}$ given by

$$\mathbf{P}^T\mathbf{V}_t\mathbf{F}_{K_0} = \mathbf{Q}_a\mathbf{R}_a, \tag{23}$$

where $\mathbf{Q}_a \in \mathbb{C}^{M_{t,R} \times K_0}$ contains orthonormal columns, and $\mathbf{R}_a \in \mathbb{C}^{K_0 \times K_0}$ is upper triangular and full rank. Substituting (22) and (23) into (21), we have

$$\begin{aligned}\mu(V) &= \frac{L}{K_0} \sup_{l \in \mathbb{N}_L^+} \mathbf{s}_l^T\mathbf{R}_a\left(\mathbf{R}_a^H\mathbf{R}_a\right)^{-1}\mathbf{R}_a^H\mathbf{s}_l^* \\ &= \frac{L}{K} \sup_{l \in \mathbb{N}_L^+} \mathbf{s}_l^T\mathbf{s}_l^* = \frac{L}{K} \sup_{l \in \mathbb{N}_L^+} \|\mathbf{s}_l\|_2^2\end{aligned} \tag{24}$$

where $\mathbf{s}_l \triangleq \mathbf{Q}_a^T\mathbf{S}_{\cdot l}$, and the second equality holds because $\mathbf{R}_a$ is invertible. Based on [78, Theorem 3], if $M_{t,R} = \mathcal{O}(L/\ln L)$, the entries of $\mathbf{S}$ can be approximated by i.i.d Gaussian random variables with distribution $\mathcal{CN}(0, 1/L)$. Since $\mathbf{Q}_a$ has orthonormal columns, $\mathbf{s}_l \in \mathbb{C}^{K_0}, \forall l \in \mathbb{N}_L^+$ also contains i.i.d Gaussian random variable with distribution $\mathcal{CN}(0, 1/L)$, and $L\|\mathbf{s}_l\|_2^2$ is distributed according to $\chi_{K_0}^2$. Based on Lemma 2 setting $t = \sqrt{6\ln L}$, it holds that

$$\Pr\left(L\|\mathbf{s}_l\|_2^2 \geq K_0 + 2\sqrt{3K_0\ln L} + 6\ln L\right) \leq L^{-3}. \tag{25}$$

Applying the union bound, we have

$$\Pr\left(\sup_{l \in \mathbb{N}_L^+} \|\mathbf{s}_l\|_2^2 \geq \frac{K_0 + 2\sqrt{3K_0\ln L} + 6\ln L}{L}\right) \leq L^{-2}. \tag{26}$$

Combining (24) and (26) gives

$$\Pr\left(\mu(V) \geq \frac{K_0 + 2\sqrt{3K\ln L} + 6\ln L}{K_0}\right) \leq L^{-2}. \tag{27}$$

From the derivation, the bound on $\mu(V)$ holds for any target angles, array geometry, and precoding matrix $\mathbf{P}$ as long as $\mathbf{P}^T\mathbf{V}_t\mathbf{F}_{K_0}$ is with full column rank K_0. Theorem 1 is proved. ■

Appendix B

Derivation of ESP and EIP in (8) and (9)

The derivation of ESP is shown as bellow

$$\begin{aligned}
\text{ESP} &\triangleq \mathbb{E}\left\{\text{Tr}\left(\mathbf{\Omega}\circ(\mathbf{DPS})\left(\mathbf{\Omega}\circ(\mathbf{DPS})^H\right)\right)\right\}\\
&= \mathbb{E}\left\{\text{Tr}\left\{\left[\sum\nolimits_k \beta_k\mathbf{\Omega}\circ(\mathbf{D}_k\mathbf{PS})\right]\left[\sum\nolimits_k \beta_k\mathbf{\Omega}\circ(\mathbf{D}_k\mathbf{PS})^H\right]\right\}\right\}\\
&= \mathbb{E}\left\{\text{Tr}\left\{\sum\nolimits_k\sum\nolimits_j \beta_k\beta_j\mathbf{\Omega}\circ(\mathbf{D}_k\mathbf{PS})\left[\mathbf{\Omega}\circ(\mathbf{D}_j\mathbf{PS})^H\right]\right\}\right\}\\
&= \text{Tr}\left\{\sum\nolimits_k\sum\nolimits_j \mathbb{E}\{\beta_k\beta_j\}\left[\sum\nolimits_l \mathbf{\Delta}_l\mathbf{D}_k\mathbf{P}\mathbb{E}\{\mathbf{s}_l\mathbf{s}_l^H\}\mathbf{P}^H\mathbf{D}_j^H\mathbf{\Delta}_l\right]\right\}\\
&\overset{(a)}{=} \text{Tr}\left\{\sum\nolimits_k \sigma_{\beta_k}^2\left[\sum\nolimits_l \mathbf{\Delta}_l\mathbf{D}_k\mathbf{\Phi}\mathbf{D}_k^H\mathbf{\Delta}_l\right]\right\}\\
&\overset{(b)}{=} \text{Tr}\left(\sum\nolimits_k \sigma_{\beta_k}^2\mathbf{\Delta}\mathbf{D}_k\mathbf{\Phi}\mathbf{D}_k^H\right) = \text{Tr}\left(\mathbf{\Phi}\sum\nolimits_k \sigma_{\beta_k}^2\mathbf{D}_k^H\mathbf{\Delta}\mathbf{D}_k\right)\\
&= \text{Tr}\left(\mathbf{\Phi}\sum\nolimits_k \sigma_{\beta_k}^2\mathbf{v}_t^*(\theta_k)\mathbf{v}_r^H(\theta_k)\mathbf{\Delta}\mathbf{v}_r(\theta_k)\mathbf{v}_t^T(\theta_k)\right)\\
&\overset{(c)}{=} pLM_{r,R}\text{Tr}\left(\mathbf{\Phi}\sum\nolimits_k \sigma_{\beta_k}^2\mathbf{v}_t^*(\theta_k)\mathbf{v}_t^T(\theta_k)\right)\\
&= pLM_{r,R}\text{Tr}\left(\mathbf{\Phi}\mathbf{D}_t\right)
\end{aligned}$$

where $\mathbf{D}_k \triangleq \mathbf{v}_r(\theta_k)\mathbf{v}_t^T(\theta_k)$, $\mathbf{s}_l \triangleq \mathbf{s}(l)$. (a) follows from the fact that $\mathbb{E}\{\beta_k\beta_j\} = \delta_{jk}\sigma_{\beta_k}^2$; (b) follows from the fact that $\mathbf{\Delta}_l = \mathbf{\Delta}_l\mathbf{\Delta}_l$ and $\mathbf{\Delta} = \sum_{l=1}^L \mathbf{\Delta}_l$; (c) follows from the fact that $\mathbf{v}_r^H(\theta_k)\mathbf{\Delta}\mathbf{v}_r(\theta_k) = \|\mathbf{\Delta}\|_1 = pLM_{r,R}$. The derivation for EIP is similar and is omitted for brevity.

Appendix C

Proof of Proposition 2

Proof: If $C < C_{\max}(P_C)$, the feasible set for $\{\mathbf{R}_{xl}\}$ determined by constraints in (10a) and (10b) $\mathcal{F}_{\{\mathbf{R}_{xl}\}}$ is nonempty as long as $\text{Tr}(\mathbf{\Phi})$ is sufficiently small. If $\xi \leq \xi_{\max}$, the feasible set for $\mathbf{\Phi}$ determined by constraints in (10c) $\mathcal{F}_{\mathbf{\Phi}1}$ is nonempty and has no restriction on $\text{Tr}(\mathbf{\Phi})$. If $\mathbf{\Phi} \in \mathcal{F}_{\mathbf{\Phi}1}$, then $\alpha\mathbf{\Phi} \in \mathcal{F}_{\mathbf{\Phi}1}, \forall\alpha > 0$. The overall feasible set for $\mathbf{\Phi}$, $\mathcal{F}_{\mathbf{\Phi}}$, is the intersection of feasible sets determined by (10a), (10b) and (10c). $\mathcal{F}_{\mathbf{\Phi}}$ is nonempty as long as $\mathcal{F}_{\mathbf{\Phi}1}$ and $\mathcal{F}_{\{\mathbf{R}_{xl}\}}$ are nonempty because we can choose any $\mathbf{\Phi} \in \mathcal{F}_{\mathbf{\Phi}1}$ and scale it down to make $(\mathbf{P}_1)$ feasible. The claim is proven. ■

Appendix D

Proof of Lemma 1

Proof: For simplicity of notation, we denote that $\mathbf{X} \triangleq \mathbf{G}_1\mathbf{\Phi}\mathbf{G}_1^H + \sigma_C^2\mathbf{I} \succ 0$ and $\mathbf{Y} \triangleq \mathbf{H}\mathbf{R}_{xl}\mathbf{H}^H \succeq 0$. It is easy to see that $\mathbf{A}$ is Hermitian because both $\mathbf{X}^{-1}$ and $(\mathbf{X}+\mathbf{Y})^{-1}$ are Hermitian. It is sufficient to show that

$\mathbf{Z} \triangleq \mathbf{X}^{-1} - (\mathbf{X}+\mathbf{Y})^{-1}$ is positive semidefinite. We have that

$$\mathbf{X}^{-1} - (\mathbf{X}+\mathbf{Y})^{-1} = \mathbf{X}^{-1}\mathbf{Y}(\mathbf{X}+\mathbf{Y})^{-1},$$

which could be shown by right multiplying $(\mathbf{X}+\mathbf{Y})$ on both sides of the equality. Since $\mathbf{X}$, $\mathbf{Y}$ and $\mathbf{Z}$ are Hermitian, we have

$$\mathbf{Z} = \mathbf{X}^{-1}\mathbf{Y}(\mathbf{X}+\mathbf{Y})^{-1} = (\mathbf{X}+\mathbf{Y})^{-1}\mathbf{Y}\mathbf{X}^{-1}.$$

Since $(\mathbf{X}+\mathbf{Y})^{-1}$ is invertible, there exists a unique positive definite matrix $\mathbf{V}$, such that $(\mathbf{X}+\mathbf{Y})^{-1} = \mathbf{V}^2$. Simple algebra manipulation shows that

$$\begin{aligned}\mathbf{V}^{-1}\mathbf{Z}\mathbf{V}^{-1} &= (\mathbf{V}^{-1}\mathbf{X}^{-1}\mathbf{V}^{-1})(\mathbf{V}\mathbf{Y}\mathbf{V}) \\ &= (\mathbf{V}\mathbf{Y}\mathbf{V})(\mathbf{V}^{-1}\mathbf{X}^{-1}\mathbf{V}^{-1}),\end{aligned}$$

i.e., $\mathbf{V}^{-1}\mathbf{Z}\mathbf{V}^{-1}$ is a product of two commutable positive semidefinite matrices $\mathbf{V}^{-1}\mathbf{X}^{-1}\mathbf{V}^{-1}$ and $\mathbf{V}\mathbf{Y}\mathbf{V}$. Therefore, $\mathbf{V}^{-1}\mathbf{Z}\mathbf{V}^{-1}$ and thus $\mathbf{Z}$ is positive semidefinite. We prove that $\mathbf{A}_l$ is semidefinite. Further, $\mathbf{A}$ is also semidefinte because it is the sum of L semidefinite matrices. ■

APPENDIX E
PROOF OF PROPOSITION 4

Proof: Problem (18) is an SDP, whose Karush-Kuhn-Tucker (KKT) conditions are given as

$$\mathbf{\Psi} + \lambda_2\mathbf{D}_t + \sum_{k=1}^{K}\nu_k\mathbf{V}_k = \mathbf{I} + \lambda_1\mathbf{A} + \lambda_2\gamma\mathbf{C}_t + \sum_{k=1}^{K}\nu_k\xi\mathbf{I} \tag{28a}$$

$$\mathbf{\Psi}\mathbf{\Phi} = \mathbf{0} \tag{28b}$$

$$\mathbf{\Psi} \succeq 0, \mathbf{\Phi} \succeq 0, \lambda_1 \geq 0, \lambda_2 \geq 0, \{\nu_k\} \geq 0 \tag{28c}$$

$$\mathrm{Tr}(\mathbf{\Phi}\mathbf{D}_t) \geq \gamma\mathrm{Tr}(\mathbf{\Phi}\mathbf{C}) + \gamma\rho \tag{28d}$$

$$\mathrm{Tr}(\mathbf{\Phi}\mathbf{V}_k) \geq 0, \forall k \in \mathbb{N}_K^+ \tag{28e}$$

where $\mathbf{\Psi} \succeq 0, \lambda_1 \geq 0, \lambda_2 \geq 0$, and $\{\nu_k\} \geq 0$ are dual variables. We can rewrite (28a) as follows

$$\begin{aligned}&\mathrm{rank}(\mathbf{\Psi}) + \mathrm{rank}\left(\lambda_2\mathbf{D}_t + \sum_{k=1}^{K}\nu_k\mathbf{v}_t^*(\theta_k)\mathbf{v}_t^T(\theta_k)\right) \\ &\geq \mathrm{rank}\left(\mathbf{I} + \lambda_1\mathbf{A} + \lambda_2\gamma\mathbf{C}_t + \sum_{k=1}^{K}\nu_k\xi\mathbf{I}\right).\end{aligned} \tag{29}$$

Recall that $\mathbf{D}_t = \sum_k \sigma_{\beta_k}^2\mathbf{v}_t^*(\theta_k)\mathbf{v}_t^T(\theta_k)$. It is clear to see that $\lambda_2\mathbf{D}_t + \sum_{k=1}^{K}\nu_k\mathbf{v}_t^*(\theta_k)\mathbf{v}_t^T(\theta_k)$ has rank at most K. Since $\mathbf{A}$ and $\mathbf{C}$ are positive semidefinite, the matrix on right hand side of (29) has full rank. Therefore, $\mathrm{rank}(\mathbf{\Psi})$ is not smaller than $M_{t,R} - K$. From (28b) and (28d) we conclude that any optimal solution $\mathbf{\Phi}$ must have rank at most K.

The second claim asserts that if there are multiple solutions with rank K, they have the same range space. This can be proved using contradiction. Suppose that $\mathbf{\Phi}_1^*$ and $\mathbf{\Phi}_2^*$ are rank-K solutions of (18) and $\mathcal{R}(\mathbf{\Phi}_1^*) \neq \mathcal{R}(\mathbf{\Phi}_2^*)$. Based on convex theory, any convex combination of $\mathbf{\Phi}_1^*$ and $\mathbf{\Phi}_2^*$, saying $\mathbf{\Phi}_3^* \triangleq \alpha\mathbf{\Phi}_1^* + (1-\alpha)\mathbf{\Phi}_2^*, \forall\alpha \in (0,1)$,

is also a solution of (18). However, $\mathbf{\Phi}_3^*$ is with rank at least $K+1$, which contradicts the fact that any solution must have rank at most K. The third claim could also be proved using contradiction. Suppose that $\mathbf{\Phi}_1^*$ and $\mathbf{\Phi}_2^*$ are respectively rank-K solution and solution with rank smaller than K, and $\mathcal{R}(\mathbf{\Phi}_2^*) \setminus \mathcal{R}(\mathbf{\Phi}_1^*)$ is nonempty. Then any convex combination of $\mathbf{\Phi}_1^*$ and $\mathbf{\Phi}_2^*$, saying $\mathbf{\Phi}_3^* \triangleq \alpha\mathbf{\Phi}_1^* + (1-\alpha)\mathbf{\Phi}_2^*, \forall \alpha \in (0,1)$, is also a solution of (18). However, $\mathbf{\Phi}_3^*$ is again with rank at least $K+1$, which contradicts the fact that any solution must have rank at most K.

The last claim on the solutions of (16) and (17) follows from Proposition 3. ■

REFERENCES

[1] "Realizing the full potential of government-held spectrum to spur economic growth," Tech. Rep., The Presidents Council of Advisors on Science and Technology (PCAST), July 2012.

[2] "FCC proposes innovative small cell use in 3.5 GHz band," Tech. Rep., Federal Communications Commission (FCC), December 2012.

[3] Locke, G. and Strickling, L. E., "An assessment of the near-term viability of accommodating wireless broadband systems in the 1675-1710 MHz, 1755-1780 MHz, 3500-3650 MHz, and 4200-4220 MHz, 4380-4400 MHz bands," Technical Report TR-13-490, US Dept. of Commerce, the National Telecommunications and Information Administration, 2012.

[4] "Radar spectrum regulatory overview," *[online] 2013*, http://www.darpa.mil/WorkArea/DownloadAsset.aspx?id=2147486331, (Accessed: July 2014).

[5] Sanders, F. H., Sole, R. L., Carroll, J. E., Secrest, G. S., and Allmon, T. L., "Analysis and resolution of RF interference to radars operating in the band 2700–2900 MHz from broadband communication transmitters," Technical Report TR-13-490, US Dept. of Commerce, NTIA, 2012.

[6] Lackpour, A., Luddy, M., and Winters, J., "Overview of interference mitigation techniques between WiMAX networks and ground based radar," in *20th Annual Wireless and Optical Communications Conference*, April 2011, pp. 1–5.

[7] Sodagari, S., Khawar, A., Clancy, T. C., and McGwier, R., "A projection based approach for radar and telecommunication systems coexistence," in *IEEE Global Telecommunication Conference*, Dec 2012, pp. 5010–5014.

[8] Sanders, F. H., Sole, R. L., Bedford, B. L., Franc, D., and Pawlowitz, T., "Effects of RF interference on radar receivers," in *NTIA Report TR-06- 444, U.S. DEPARTMENT OF COMMERCE*.

[9] Bell, M. R., Devroye, N., Erricolo, D., Koduri, T., Rao, S., and Tuninetti, D., "Results on spectrum sharing between a radar and a communications system," in 2014 International Conference on Electromagnetics in Advanced Applications (ICEAA), 2014, pp. 826–829.

[10] Zhao, Q. and Sadler, B. M., "A survey of dynamic spectrum access," *IEEE Signal Processing Magazine*, vol. 24, no. 3, pp. 79–89, May 2007.

[11] Hossain, E., Niyato, D., and Han, Z., *Dynamic spectrum access and management in cognitive radio networks*, Cambridge university press, 2009.

[12] Wang, L. S., McGeehan, J. P., Williams, C., and Doufexi, A., "Application of cooperative sensing in radar-communications coexistence," *IET Communications*, vol. 2, no. 6, pp. 856–868, July 2008.

[13] Bhat, S. S., Narayanan, R. M., and Rangaswamy, M., "Bandwidth sharing and scheduling for multimodal radar with communications and tracking," in *IEEE Sensor Array and Multichannel Signal Processing Workshop*, June 2012, pp. 233–236.

[14] Saruthirathanaworakun, R., Peha, J. M., and Correia, L. M., "Opportunistic sharing between rotating radar and cellular," *IEEE Journal on Selected Areas in Communications*, vol. 30, no. 10, pp. 1900–1910, 2012.

[15] Surender, S. C., Narayanan, R. M., and Das, C. R., "Performance analysis of communications & radar coexistence in a covert UWB OSA system," in *IEEE Global Telecommunications Conference*, 2010, pp. 1–5.

[16] Gogineni, S., Rangaswamy, M., and Nehorai, A., "Multi-modal OFDM waveform design," in *IEEE Radar Conference*, April 2013, pp. 1–5.

[17] Turlapaty, A. and Jin, Y., "A joint design of transmit waveforms for radar and communications systems in coexistence," in *IEEE Radar Conference*, 2014, pp. 0315–0319.

[18] Aubry, A., A., D. M., M., P., and Farina, A., "Radar waveform design in a spectrally crowded environment via nonconvex quadratic optimization," *IEEE Transactions on Aerospace and Electronic Systems*, vol. 50, no. 2, pp. 1138–1152, 2014.

[19] Aubry, A., De Maio, A., Huang, Y., Piezzo, M., and Farina, A., "A new radar waveform design algorithm with improved feasibility for spectral coexistence," *IEEE Transactions on Aerospace and Electronic Systems*, vol. 51, no. 2, pp. 1029–1038, April 2015.

[20] Huang, K., Bica, M., Mitra, U., and Koivunen, V., "Radar waveform design in spectrum sharing environment: Coexistence and cognition," in *Radar Conference (RadarCon), 2015 IEEE*. IEEE, 2015, pp. 1698–1703.

[21] Bica, M., Huang, K. W., Koivunen, V., and Mitra, U., "Mutual information based radar waveform design for joint radar and cellular communication systems," in *2016 IEEE International Conference on Acoustics, Speech and Signal Processing (ICASSP)*, March 2016, pp. 3671–3675.

[22] Babaei, A., Tranter, W. H., and Bose, T., "A practical precoding approach for radar/communications spectrum sharing," in *8th International Conference on Cognitive Radio Oriented Wireless Networks*, July 2013, pp. 13–18.

[23] Amuru, S., Buehrer, R. M., Tandon, R., and Sodagari, S., "MIMO radar waveform design to support spectrum sharing," in *IEEE Military Communication Conference*, Nov 2013, pp. 1535–1540.

[24] Khawar, A., Abdel-Hadi, A., and Clancy, T. C., "Spectrum sharing between S-band radar and LTE cellular system: A spatial approach," in *IEEE International Symposium on Dynamic Spectrum Access Networks,*, April 2014, pp. 7–14.

[25] Shahriar, C., Abdelhadi, A., and Clancy, T. C., "Overlapped-MIMO radar waveform design for coexistence with communication systems," in *IEEE Wireless Communications and Networking Conference*, 2015, pp. 223–228.

[26] Khawar, A., Abdelhadi, A., and Clancy, T. C., *MIMO Radar Waveform Design for Spectrum Sharing with Cellular Systems: A MATLAB Based Approach*, Springer, 2016.

[27] Deng, H. and Himed, B., "Interference mitigation processing for spectrum-sharing between radar and wireless communications systems," *IEEE Transactions on Aerospace and Electronic Systems*, vol. 49, no. 3, pp. 1911–1919, July 2013.

[28] Li, B. and Petropulu, A. P., "Spectrum sharing between matrix completion based MIMO radars and a MIMO communication system," in *IEEE International Conference on Acoustics, Speech and Signal Processing*, April 2015, pp. 2444–2448.

[29] Li, B., Petropulu, A. P., and Trappe, W., "Optimum co-design for spectrum sharing between matrix completion based MIMO radars and a MIMO communication system," *IEEE Transactions on Signal Processing*, vol. 64, no. 17, pp. 4562–4575, Sept 2016.

[30] Li, B. and Petropulu, A. P., "Radar precoding for spectrum sharing between matrix completion based MIMO radars and a MIMO communication system," in *IEEE Global Conference on Signal and Information Processing*, Dec 2015, pp. 737–741.

[31] Li, B., Kumar, H., and Petropulu, A. P., "A joint design approach for spectrum sharing between radar and communication systems," in *IEEE International Conference on Acoustics, Speech and Signal Processing*, March 2016, pp. 3306–3310.

[32] Li, B. and Petropulu, A. P., "MIMO radar and communication spectrum sharing with clutter mitigation," in *IEEE Radar Conference*, May 2016, pp. 1–6.

[33] Sun, S., Bajwa, W., and Petropulu, A. P., "MIMO-MC radar: A MIMO radar approach based on matrix completion," *IEEE Transactions on Aerospace and Electronic Systems*, vol. 51, no. 3, pp. 1839–1852, July 2015.

[34] Kalogerias, D. S. and Petropulu, A. P., "Matrix completion in colocated MIMO radar: Recoverability, bounds and theoretical guarantees," *IEEE Transactions on Signal Processing*, vol. 62, no. 2, pp. 309–321, Jan 2014.

[35] Sun, S. and Petropulu, A. P., "Waveform design for MIMO radars with matrix completion," *IEEE Journal of Selected Topics in Signal Processing*, vol. 9, no. 8, pp. 1400–1414, Dec 2015.

[36] Candès, E. J. and Plan, Y., "Matrix completion with noise," *Proceedings of the IEEE*, vol. 98, no. 6, pp. 925–936, June 2010.

[37] Chen, C. and Vaidyanathan, P. P., "Compressed sensing in MIMO radar," in *Asilomar Conference on Signals, Systems and Computers,*. IEEE, 2008, pp. 41–44.

[38] Yu, Y., Petropulu, A. P., and Poor, H. V., "MIMO radar using compressive sampling," *IEEE Journal of Selected Topics in Signal Processing*, vol. 4, no. 1, pp. 146–163, Feb 2010.

[39] Amin, M. G., *Compressive sensing for urban radar*, CRC Press, 2014.

[40] Richards, M. A., *Fundamentals of Radar Signal Processing*, McGraw-Hill, New York, 2005.

[41] Stoica, P., Li, J., and Xie, Y., "On probing signal design for MIMO radar," *IEEE Transactions on Signal Processing*, vol. 55, no. 8, pp. 4151–4161, 2007.

[42] Cui, G., Li, H., and Rangaswamy, M., "MIMO radar waveform design with constant modulus and similarity constraints," *IEEE Transactions*

on Signal Processing, vol. 62, no. 2, pp. 343–353, 2014.

[43] Chen, Z., Li, H., Cui, G., and Rangaswamy, M., "Adaptive transmit and receive beamforming for interference mitigation," *IEEE Signal Processing Letters*, vol. 21, no. 2, pp. 235–239, Feb 2014.

[44] Krim, H. and Viberg, M., "Two decades of array signal processing research: The parametric approach," *IEEE Signal Processing Magazine*, vol. 13, no. 4, pp. 67–94, 1996.

[45] Zyczkowski, K. and Kus, M., "Random unitary matrices," *Journal of Physics A: Mathematical and General*, vol. 27, no. 12, pp. 4235, 1994.

[46] Laurent, B. and Massart, P., "Adaptive estimation of a quadratic functional by model selection," *Annals of Statistics*, pp. 1302–1338, 2000.

[47] Candès, E. J. and Recht, B., "Exact matrix completion via convex optimization," *Foundations of Computational mathematics*, vol. 9, no. 6, pp. 717–772, 2009.

[48] "Amendment of the commissions rules with regard to commercial operations in the 3550-3650 mhz band," Tech. Rep., Fedreal Communications Commission (FCC), April 2015.

[49] Kopp, C., "Search and acquisition radars (S-band, X-band)," *Technical Report APA-TR-2009-0101, [online] 2009*, http://www.ausairpower.net/APA-Acquisition-GCI.html, (Accessed: July 2015).

[50] "Radar performance," *Radtec Engineering Inc., [online]*, http://www.radar-sales.com/PDFs/Performance_RDR\%26TDR.pdf, (Accessed: July 2015).

[51] Rappaport, T., *Wireless Communications Principles And Practice Edition*, Prentice Hall, 2001.

[52] Tse, D. and Viswanath, P., *Fundamentals of wireless communication*, Cambridge university press, 2005.

[53] Goldsmith, A., *Wireless communications*, Cambridge university press, 2005.

[54] Jover, R. P., "LTE PHY fundamentals," *[online] 2015*, http://www.ee.columbia.edu/~roger/LTE_PHY_fundamentals.pdf, (Accessed: July 2015).

[55] Innovations, T., "LTE in a nutshell: The physical layer," *White paper*, 2010.

[56] Andrews, J. G., Ghosh, A., and Muhamed, R., *Fundamentals of WiMAX: Understanding Broadband Wireless Networking*, Prentice Hall PTR, Upper Saddle River, NJ, USA, 2007.

[57] Li, B. and Petropulu, A. P., "Distributed MIMO radar based on sparse sensing: Analysis and efficient implementation," *IEEE Transactions on Aerospace and Electronic Systems*, vol. 51, no. 4, pp. 3055–3070, Oct 2015.

[58] Filo, M., Hossain, A., Biswas, A. R., and Piesiewicz, R., "Cognitive pilot channel: Enabler for radio systems coexistence," in *2nd International Workshop on Cognitive Radio and Advanced Spectrum Management*, May 2009, pp. 17–23.

[59] Rogalin, R., Bursalioglu, O. Y., and Papadopoulos, H., "Scalable synchronization and reciprocity calibration for distributed multiuser MIMO," *IEEE Transactions on Wireless Communications*, vol. 13, no. 4, pp. 1815–1831, 2014.

[60] Zhang, R. and Liang, Y., "Exploiting multi-antennas for opportunistic spectrum sharing in cognitive radio networks," *IEEE Journal of Selected Topics in Signal Processing*, vol. 2, no. 1, pp. 88–102, Feb 2008.

[61] Zhang, R., Liang, Y., and Cui, S., "Dynamic resource allocation in cognitive radio networks," *IEEE Signal Processing Magazine*, vol. 27, no. 3, pp. 102–114, May 2010.

[62] Kim, S. J. and Giannakis, G. B., "Optimal resource allocation for MIMO Ad Hoc cognitive radio networks," *IEEE Transactions on Information Theory*, vol. 57, no. 5, pp. 3117–3131, May 2011.

[63] Lu, L., Zhou, X., Onunkwo, U., and Li, G. Y., "Ten years of research in spectrum sensing and sharing in cognitive radio.," *EURASIP J. Wireless Comm. and Networking*, vol. 2012, pp. 28, 2012.

[64] Phan, K. T., Vorobyov, S. A., Sidiropoulos, N. D., and Tellambura, C., "Spectrum sharing in wireless networks via QoS-aware secondary multicast beamforming," *IEEE Transactions on signal processing*, vol. 57, no. 6, pp. 2323–2335, 2009.

[65] Du, H. and Ratnarajah, T., "Robust utility maximization and admission control for a MIMO cognitive radio network," *IEEE Transactions on Vehicular Technology*, vol. 62, no. 4, pp. 1707–1718, 2013.

[66] Hou, X. and Yang, C., "How much feedback overhead is required for base station cooperative transmission to outperform non-cooperative transmission?," in *2011 IEEE International Conference on Acoustics, Speech and Signal Processing (ICASSP)*. IEEE, 2011, pp. 3416–3419.

[67] Mudumbai, R., Barriac, G., and Madhow, U., "On the feasibility of distributed beamforming in wireless networks," *IEEE Transactions on Wireless Communications*, vol. 6, no. 5, pp. 1754–1763, 2007.

[68] Chen, C. and Vaidyanathan, P. P., "MIMO radar ambiguity properties and optimization using frequency-hopping waveforms," *IEEE*

Transactions on Signal Processing, vol. 56, no. 12, pp. 5926–5936, 2008.

[69] Diggavi, S. N. and Cover, T. M., "The worst additive noise under a covariance constraint," *IEEE Transactions on Information Theory*, vol. 47, no. 7, pp. 3072–3081, Nov 2001.

[70] Chen, C. and Vaidyanathan, P. P., *MIMO Radar Spacetime Adaptive Processing and Signal Design*, pp. 235–281, John Wiley & Sons, Inc., 2008.

[71] Bhojanapalli, S. and Jain, P., "Universal matrix completion," in *Proceedings of The 31st International Conference on Machine Learning*, 2014, pp. 1881–1889.

[72] Boyd, S. and Vandenberghe, L., *Convex optimization*, Cambridge university press, 2004.

[73] Kuhn, H. W., "The Hungarian method for the assignment problem," *Naval research logistics quarterly*, vol. 2, no. 1-2, pp. 83–97, 1955.

[74] Li, Q. and Ma, W.-K., "Optimal and robust transmit designs for MISO channel secrecy by semidefinite programming," *IEEE Transactions on Signal Processing*, vol. 59, no. 8, pp. 3799–3812, 2011.

[75] Yeh, J., "Real analysis," in *Theory of measure and integration*, Theory of measure and integration. World Scientific, Singapore, 2006.

[76] "3GPP TS LTE evolved universal terrestrial radio access (E-UTRA) physical layer procedures (36.213 v8.0)," Tech. Rep., 3rd Generation Partnership Project Std, 2009.

[77] Kawser, M. T., Hamid, B., Hasan, N., Alam, M. S., and Rahman, M. M., "Downlink SNR to CQI mapping for different multipleantenna techniques in LTE," *International Journal of Information and Electronics Engineering*, vol. 2, no. 5, pp. 757, 2012.

[78] Jiang, T., "How many entries of a typical orthogonal matrix can be approximated by independent normals?," *The Annals of Probability*, vol. 34, no. 4, pp. 1497–1529, 2006.

Bo Li (S'13) received his B.E. degree in communication engineering from Lanzhou University, China, in 2009, the M.S. in in electrical engineering from Peking University, China, in 2012, and the Ph.D. degree at the Department of Electrical & Computer Engineering, Rutgers, The State University of New Jersey, USA in 2016. Now he works at Qualcomm R&D, San Diego, CA, USA as a research engineer. His research interests are in signal processing for MIMO radar and wireless communication systems, including compressive sensing and matrix completion based MIMO radar, spectrum sharing in cooperative radar and communication systems.

Athina P. Petropulu (F'08) received her undergraduate degree from the National Technical University of Athens, Greece, and the M.Sc. and Ph.D. degrees from Northeastern University, Boston MA, all in Electrical and Computer Engineering. Since 2010, she is Professor of the Electrical and Computer Engineering (ECE) Department at Rutgers, having served as chair of the department during 2010-2016. Before that she was faculty at Drexel University. She held Visiting Scholar appointments at SUPELEC, Universite Paris Sud (1999-2000), Princeton University (2006-2007) and University of Southern California (2016-2017). Dr. Petropulu's research interests span the area of statistical signal processing, wireless communications, signal processing in networking, physical layer security, and radar signal processing. Her research has been funded by various government industry sponsors including the National Science Foundation, the Office of Naval research, the US Army, the National Institute of Health, the Whitaker Foundation, Lockheed Martin.

Dr. Petropulu is Fellow of IEEE and recipient of the 1995 Presidential Faculty Fellow Award given by NSF and the White House. She has served as Editor-in-Chief of the IEEE Transactions on Signal Processing (2009-2011), IEEE Signal Processing Society Vice President-Conferences (2006-2008), and member-at-large of the IEEE Signal Processing Board of Governors. She was the General Chair of the 2005 International Conference on Acoustics Speech and Signal Processing (ICASSP-05), Philadelphia PA. In 2005 she received the IEEE Signal Processing Magazine Best Paper Award, and in 2012 the IEEE Signal Processing Society Meritorious Service Award for "exemplary service in technical leadership capacities". She was IEEE Distinguished Lecturer for the Signal Processing Society for 2017-2018.

More info on her work can be found at www.ece.rutgers.edu/~cspl

LIST OF FIGURES

1 A MIMO communication system sharing spectrum with a colocated MIMO radar system 9

2 The proposed spectrum sharing architecture. The cooperation is coordinated by the control center, a node with high computing power that also serves as the radar fusion center. The control center collects information from radar and communication systems, computes jointly optimal signaling schemes for both systems and sends each scheme back to the corresponding system. 9

3 TDM based CSI estimation and feedback and reception of design results from the control center. . . 10

4 The radar transmit beampattern and the MUSIC spatial pseudo-spectrum for MIMO-MC radar and communication spectrum sharing. $M_{t,R} = M_{r,R} = 16, M_{t,C} = M_{r,C} = 4$. The true positions of the targets and clutters are labeled using solid and dashed vertical lines, respectively. CNR=30 dB. 20

5 Comparison of spectrum sharing with different levels of cooperation between the MIMO-MC radar and the communication system under different P_R. $M_{t,R} = M_{r,R} = 16, M_{t,C} = M_{r,C} = 4$. 22

6 Comparison of spectrum sharing with adaptive and constant-rate communication transmissions under different levels of variance of the interference channel from the communication transmitter to the radar receiver. $M_{t,R} = 16, M_{r,R} = M_{t,C} = 8, M_{r,C} = 2$. 23

7 Comparison of spectrum sharing with traditional MIMO radars and MIMO-MC radars with different subsampling rates p. $M_{t,R} = 16, M_{r,R} = M_{t,C} = 8, M_{r,C} = 2$. 23